

## The North American upper mantle: Density, composition, and evolution

Walter D. Mooney<sup>1</sup> and Mikhail K. Kaban<sup>2</sup>

Received 11 January 2010; revised 3 June 2010; accepted 8 July 2010; published 31 December 2010.

[1] The upper mantle of North America has been well studied using various seismic methods. Here we investigate the density structure of the North American (NA) upper mantle based on the integrative use of the gravity field and seismic data. The basis of our study is the removal of the gravitational effect of the crust to determine the mantle gravity anomalies. The effect of the crust is removed in three steps by subtracting the gravitational contributions of (1) topography and bathymetry, (2) low-density sedimentary accumulations, and (3) the three-dimensional density structure of the crystalline crust as determined by seismic observations. Information regarding sedimentary accumulations, including thickness and density, are taken from published maps and summaries of borehole measurements of densities; the seismic structure of the crust is based on a recent compilation, with layer densities estimated from *P*-wave velocities. The resultant mantle gravity anomaly map shows a pronounced negative anomaly (−50 to −400 mGal) beneath western North America and the adjacent oceanic region and positive anomalies (+50 to +350 mGal) east of the NA Cordillera. This pattern reflects the well-known division of North America into the stable eastern region and the tectonically active western region. The close correlation of large-scale features of the mantle anomaly map with those of the topographic map indicates that a significant amount of the topographic uplift in western NA is due to buoyancy in the hot upper mantle, a conclusion supported by previous investigations. To separate the contributions of mantle temperature anomalies from mantle compositional anomalies, we apply an additional correction to the mantle anomaly map for the thermal structure of the uppermost mantle. The thermal model is based on the conversion of seismic shear-wave velocities to temperature and is consistent with mantle temperatures that are independently estimated from heat flow and heat production data. The thermally corrected mantle density map reveals density anomalies that are chiefly due to compositional variations. These compositional density anomalies cause gravitational anomalies that reach ~250 mGal. A pronounced negative anomaly (−50 to −200 mGal) is found over the Canadian shield, which is consistent with chemical depletion and a corresponding low density of the lithospheric mantle, also referred to as the mantle tectosphere. The strongest positive anomaly is coincident with the Gulf of Mexico and indicates a positive density anomaly in the upper mantle, possibly an eclogite layer that has caused subsidence in the Gulf. Two linear positive anomalies are also seen south of 40°N: one with a NE-SW trend in the eastern United States, roughly coincident with the Grenville-Appalachians, and a second with a NW-SE trend beneath the states of Texas, New Mexico, and Colorado. These anomalies are interpreted as being due to (1) the presence of remnants of an oceanic slab in the upper mantle beneath the Grenville-Appalachian suture and (2) mantle thickening caused by a period of shallow, flat subduction during the Laramie orogeny, respectively. Based on these geophysical results, the evolution of the NA upper mantle is depicted in a series of maps and cartoons that display the primary processes that have formed and modified the NA crust and lithospheric upper mantle.

**Citation:** Mooney, W. D., and M. K. Kaban (2010), The North American upper mantle: Density, composition, and evolution, *J. Geophys. Res.*, 115, B12424, doi:10.1029/2010JB000866.

<sup>1</sup>U.S. Geological Survey, Menlo Park, California, USA.

<sup>2</sup>GeoForschungsZentrum, Potsdam, Germany.

### 1. Introduction

[2] The North American (NA) continent has evolved over the past 4 billion years (Ga) through a series of geological



**Figure 1.** Simplified basement geologic province map of North America [after *Hoffman, 1988; Karlstrom et al., 2004; Whitmeyer and Karlstrom, 2007*]. This study is focused on the determination of the density of the underlying upper mantle and on the processes that have formed and modified the mantle.

processes, including accretion, rifting, and lateral terrain translation, that are common to all large continents. The growth of the NA continent is evidenced by the existence of Archean cratonic blocks that are surrounded by accreted Proterozoic terrains, which in turn are bounded by Phanerozoic accretionary belts (Figure 1). The growth of Precambrian North America is summarized by *Hoffman* [1988, 1989a, 1989b, 1997], *Williams et al.* [1991], and *Karlstrom et al.* [1999, 2001], who document the growth of North America by the accretion of Proterozoic terrains to the southern edge of Laurentia from 1.8 to 0.8 Ga during the creation and dispersal of the supercontinent Rodinia. Important processes

occurred during the Phanerozoic as well, with the accretion of the Appalachian Mountains on the east coast [*Hatcher, 1989; Thomas, 1989*] and the formation of the Western Cordillera, which extends from Mexico to Alaska [*Christiansen and Lipman, 1972; Oldow et al., 1989; Burchfiel et al., 1992; Dickinson, 2004*]. The Laramide orogeny (55 Ma) played a major role in forming the present-day topography of the western United States and has been widely attributed to flat subduction and, later, rollback by the east-dipping Farallon slab [*Dickinson and Snyder, 1978; Bird, 1984, 1988*]. An alternative model with west-dipping subduction has been proposed by *Hildebrand* [2009]. North America thus con-

sists of a Precambrian core that is flanked by Phanerozoic orogenic belts.

[3] Intensive geophysical studies of the crust and upper mantle of North America began in the 1960s. The basic outline consists of a 35–45 km thick crust beneath the Precambrian core and a 25–35 km thick crust within much of the western Cordillera and beneath the eastern coastal plains [Mooney and Braile, 1989; Chulick and Mooney, 2002]. The NA upper mantle was first investigated using seismic surface waves, which defined higher shear-wave velocities in the Precambrian core and lower velocities in the tectonically active west [i.e., Dorman, 1969; Burdick and Helmsberger, 1978; Iyer and Hitchcock, 1989].

[4] The increasing number of seismic stations within North America and the development of techniques for seismic tomographic imaging of the upper mantle have led to rapid advances in resolution of the structure of the upper mantle [Grand, 1994; Li and Romanowicz, 1996; Grand et al., 1997; Van der Lee and Nolet, 1997a, 1997b; Grand, 2002; Godey et al., 2003; Zhao, 2004; Zhou et al., 2006; Marone and Romanowicz, 2007; Marone et al., 2007; Nettles and Dziewonski, 2008; Bedle and Van der Lee, 2009]. These studies have demonstrated that the Canadian shield, particularly the Archean Superior province, has a high-velocity root that extends to a depth of 220+ km, while the western portion of the continent has one of the strongest low-velocity anomalies imaged under any continental region worldwide.

[5] There have been two other notable seismic observations of properties of the NA upper mantle. The first is that of azimuthal seismic anisotropy, as evidenced by shear-wave splitting [Vinnik et al., 1984; Silver and Chan, 1991; Silver, 1996; Bostock et al., 1997], and radial anisotropy, as evidenced by Rayleigh and Love wave dispersion [e.g., Marone et al., 2007]. It is generally agreed that this anisotropy is due to the alignment of the crystallographic axes of olivine within the upper mantle. While this observation is important for deciphering the deformation history of the lithosphere, it has no relation to the density structure of the upper mantle as determined here. However, we return to this observation when discussing the evolution of the NA upper mantle. The second notable seismic property observation is based on near-vertical seismic reflection profiling that documents both steeply dipping and near-horizontal seismic reflections within the upper mantle [e.g., Cook et al., 1999]. These seismic reflections provide strong evidence for the processes of plate convergence and subduction during the Precambrian.

[6] Gravity data provide valuable constraints on the physical state of the lithosphere that are complementary to the seismic data. For example, density variations within the lithosphere and sublithospheric mantle often control surface elevation. Seismic data alone do not provide sufficient information about the density structure of the upper mantle, because seismic  $P$  and seismic  $S$  velocities are controlled by a number of factors including composition, temperature, and volatile content. A clear example of the ambiguity of seismic models when considered alone is cratonic roots. These are characterized by strong positive lithospheric velocity anomalies but have near-zero density anomalies because low temperatures are compensated by compositional differences [e.g., Jordan, 1978, 1988; Boyd, 1989; Kaban et al., 2003].

[7] Dorman and Lewis [1970a, 1970b, 1972] were the first to calculate an isostatic model for North America based on cross-spectral analysis of the gravity and topography data. Simpson et al. [1986] presented an isostatic gravity anomaly map for the conterminous United States that finds frequent use in studies of structure at near-surface. However, it is not possible to use gravity data alone to estimate mantle structure, since the observed gravity field is an integral of the entire subsurface volume. The crust, being the most heterogeneous layer, often masks the effects of deeper layers. Therefore, the first step for an investigation of upper mantle density structure is the application of a correction for the crustal contribution. Recent gravity models for the uppermost mantle of North America include 2D modeling along seismic profiles [e.g., Snelson et al., 1998, Romanayuk et al., 2007] and 3D models for the western part of the continent [Kaban and Mooney, 2001].

[8] Perry et al. [2003] used gravity and seismic data to determine the thermochemical structure of the mantle beneath the NA craton. To resolve the density heterogeneity of the mantle, they have corrected the observed gravity field for the crustal effect estimated based on a  $5^\circ \times 5^\circ$  model. This model is based on the CRUST5.1 data [Mooney et al., 1998] corrected with the Lithoprobe results for Canada [Perry et al., 2002]. A global tomography model of Grand et al. [1997] was employed to constrain the thermal structure of the mantle. It was demonstrated that the inferred density heterogeneity of the mantle requires simultaneous anomalies in temperature and composition. According to the model of Perry et al. [2003], the NA lithosphere is basically divided in two parts: the upper mantle under the central-northeastern portion is characterized by strong basalt depletion and corresponding decrease in density, while the upper mantle structure in the southwestern portion is primarily controlled by temperature variations. Because of insufficient resolution of the initial data (both crustal and tomography models), the model of Perry et al. [2003] could not provide a higher resolution. Recently available data sets provide a possibility to improve this model.

[9] The available knowledge of the crustal structure of North America [cf. Chulick and Mooney, 2002], which is based on 1400 active and passive seismic source determinations, provides a good starting point to create a detailed density model of the NA crust, from which the upper mantle density structure can then be determined. Recently, Hasterok and Chapman [2007] used NA gravity and geothermal data to investigate the density structure of the upper mantle based on the isostatic approach. This approach is similar to one that was proposed by Artemjev and Kaban [1986] and applied by Mooney and Vidale [2003]. It is based on the assumption that a lithospheric column is in isostatic equilibrium. Therefore, if one has constraints on the density structure of the crust it is possible to calculate the density in the mantle that provides isostatic equilibrium of the total lithospheric column. However, there are some limitations to this approach. Regional structure is sometimes perturbed from a state of isostatic balance: the structure might be supported by the strength of the lithosphere or by mantle flow (i.e., dynamically). Therefore, in general it is only possible to compare relatively large provinces, as done in the studies by Mooney and Vidale [2003] and Hasterok and Chapman [2007]. An alternative approach, applied here,

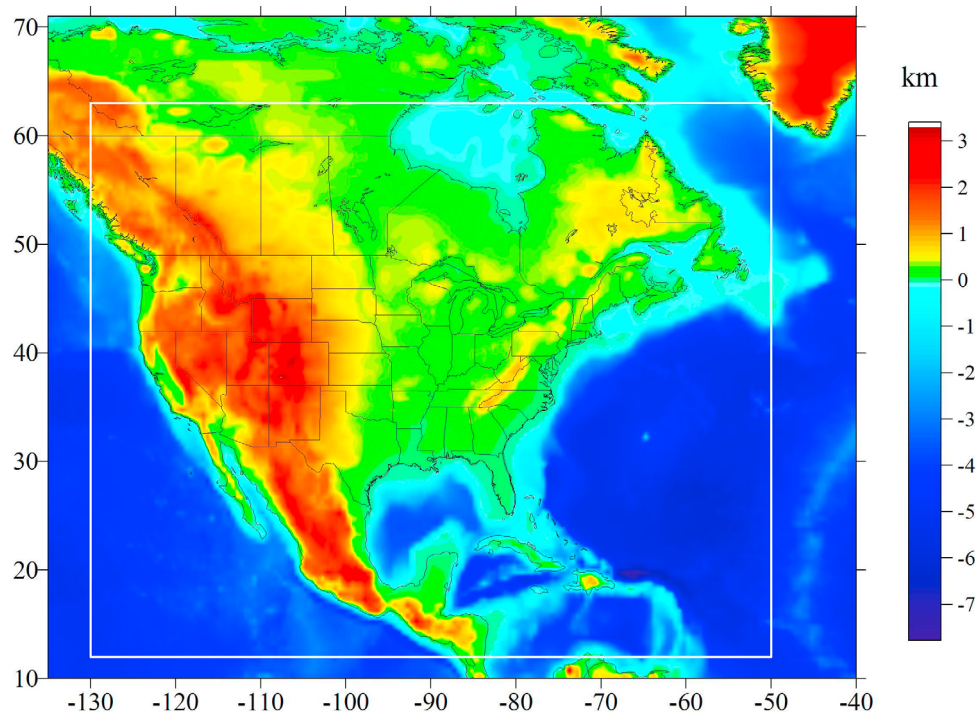


**Figure 2.** Topographic map of North America and neighboring regions. Western North America (west of  $100^{\circ}\text{E}$  at  $30^{\circ}\text{--}50^{\circ}\text{N}$ ) has a highly elevated topography. Central and eastern North America lies below 500 m, with the exception of some limited regions. This topography is accounted for when calculating the mantle gravity.

based on the modeling of the gravity field is less sensitive to these limitations. Another principal difference between our study and that of *Hasterok and Chapman* [2007] is that we primarily rely on seismic tomography to estimate mantle temperatures. This approach provides more uniform coverage than geothermal modeling, where many gaps may exist [Röhm *et al.*, 2000; Artemieva and Mooney, 2001; Goes and Van der Lee, 2002].

[10] In this paper we apply three-dimensional (3D) crustal corrections to the NA Bouguer gravity map to obtain the “crust-free,” or residual, mantle gravity anomalies. We then apply a thermal correction to the residual mantle gravity map to obtain those density anomalies due to lateral variations in composition. The thermal model is based on a high-resolution tomography model, which is also corrected for the crustal effect using the same data on the crustal structure [Goes and Van der Lee, 2002]. The mantle compositional density anomaly map provides a new view of the NA uppermost mantle.

## 2. Initial Data

### 2.1. Gravity Data

[11] The initial gravity data set consists of Bouguer gravity values with terrain corrections onshore [Godson, 1985] and free air anomaly (FAA) values offshore [Simpson *et al.*, 1986] using a grid spacing of 4 km. These data sets are based on a compilation of nearly all terrestrial gravity observations in North America. Bathymetric and topogra-

phy data (Figure 2) are taken from ETOPO2 [NOAA, 2000]. We applied a Bouguer correction to the oceanic regions by calculating the gravitational effect of bathymetry and removing it from the FAA. The resultant Bouguer gravity values interpolated onto a  $5' \times 5'$  grid are shown in Figure 3. For calculation of the residual mantle anomalies this field was averaged over  $1^{\circ} \times 1^{\circ}$  compartments and projected on the same grid as other crustal parameters (e.g., crustal thickness).

### 2.2. Thickness and Density of Sediments

[12] The first step in processing the Bouguer gravity map was to remove the effect of extensive sedimentary basins. Hydrocarbon resource exploration has involved comprehensive investigations of sedimentary basins worldwide and we have utilized this knowledge base regarding basin thickness and densities (Figure 4). A  $5' \times 5'$  digital grid of sediment thickness was prepared based on the data sources in Table 1. For the conterminous United States it is based on the compilation of *Frezon et al.* [1983] supplemented by regional sources (Table 1). For the rest of the region we used data from the *Exxon* [1985]. Extensive basins with depths of up to 15 km are located on the continental margin of the east coast of North America and in the Gulf of Mexico (Figure 4). The basins of the continental margin of the west coast are generally more shallow and narrow.

[13] It is necessary to estimate the density-depth structure of the sedimentary basins in order to calculate their gravitational effect. Of particular importance is the shallow

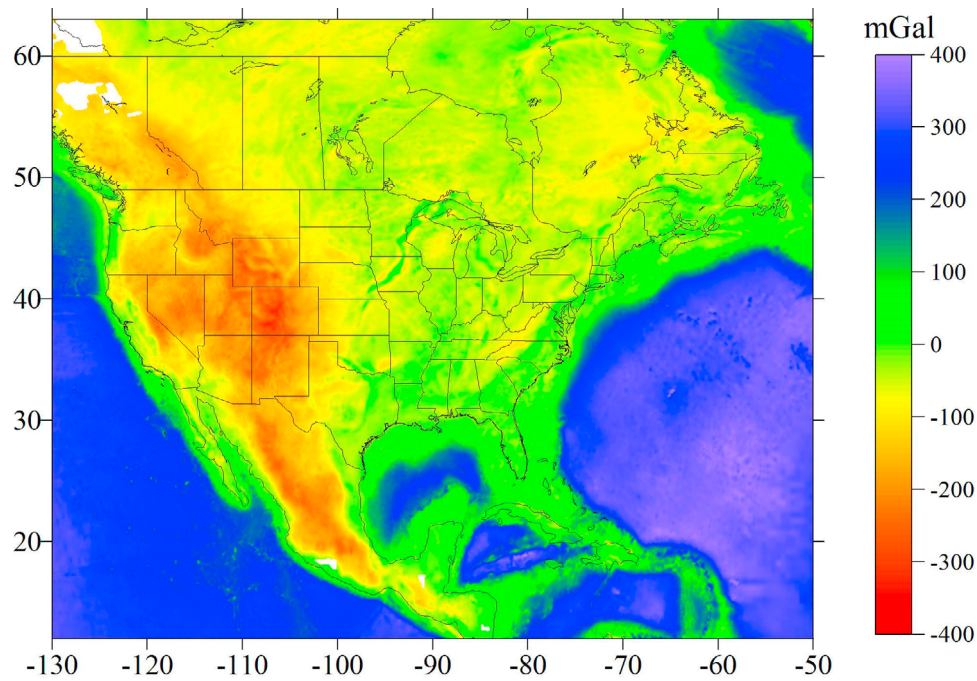


**Figure 3.** Bouguer gravity anomaly map of North America and neighboring regions [Godson, 1985; Simpson *et al.*, 1986]. These data are corrected for the gravitational contributions of low-density sediments (Figure 4), lateral variations in crustal thickness (Figure 7), and crustal density (estimated from seismic velocity), thereby yielding a mantle anomaly map.

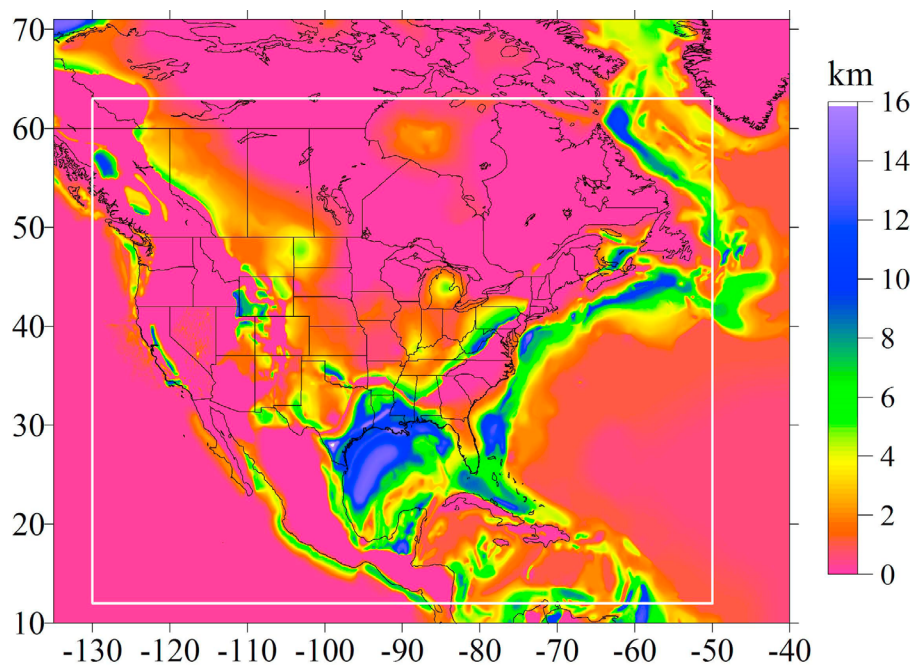


**Figure 4.** Map of sediment thickness for North America and neighboring regions. Sources are listed in Table 1. Sediments are absent or thin for large portions of the continental crust and for much of the young crust of the Pacific Ocean. The greatest sedimentary accumulations are within the Gulf of Mexico and along the East Coast of North America. The gravitational effect of these low-density sediments is removed from the observed gravity as the first step in calculating the mantle gravity field.

**Table 1.** Main Data Sources for Sediment Thickness Map<sup>a</sup>

Region	Reference
Base map for the whole area	<i>Frezon et al.</i> [1983]
Great Valley	<i>Jachens et al.</i> [1995]
Offshore basins	<i>Gardner et al.</i> [1992]
Basin and range	<i>Jachens and Moring</i> [1990]
Los Angeles basin	<i>Fuis et al.</i> [2001]; <i>Langenheim and Jachens</i> [1996]

<sup>a</sup>See Figure 4.

density structure, since for depths greater than about 6 km sedimentary rocks achieve a density that is nearly equal to that of crystalline basement rocks. We note that the density-depth structure of sedimentary basins varies considerably. For example, the Michigan and Illinois basins are characterized by dense sediments (limestone), whereas most offshore basins are filled with soft sediments. Numerous well logs provide density data to depths of 2–3 km. These data show complex variations in density with depth, including strong density contrasts [e.g., *Beyer et al.*, 1985]. However, these strong density contrasts usually have only a relatively short lateral continuity. Therefore, a reasonable approach is to construct a smooth density-depth function characterizing each type of sedimentary basin, and to ignore local and thin density anomalies. The smoothed density-depth function is based on averaged borehole data, well-determined density-compaction relations, and seismic profiling data. Thus we take into account the general properties of each basin and ignore small-scale density variations. This approach has been successfully used in previous gravity modeling of sedimentary basins [*Jachens and Moring*, 1990; *Langenheim and Jachens*, 1996; *Kaban et al.*, 1999; *Kaban and Mooney*, 2001].

[14] A set of density-depth functions for the main types of sedimentary basins in North America (Figure 5) shows that young offshore basins are filled with the least dense sediments. The well logs show that the bulk density within such basins is highly dependent on the porosity, whereas the density of individual sedimentary grains is very close to the average density of the upper crust (2600–2700 kg/m<sup>3</sup> [*McCulloh*, 1967; *Beyer et al.*, 1985; *Ocean Drilling Program*, 1994]). For these offshore basins we adopt the smooth density-depth function shown in Figure 5 [cf. *Kaban and Mooney*, 2001]. The same modeling approach is used to describe the density-depth structure of the on-shore basins (Figure 5). The gravitational effect of sediments relative to a sediment-free upper crust is shown in Figure 6.

### 2.3. Crustal Thickness and Density of the Solid Crust

[15] We have constructed a new Moho map for North America using an online database with about 1500 determinations of crustal structure [*Chulick and Mooney*, 2002]. However, even this number of data is not sufficient to construct a Moho map with 1° × 1° resolution using only simple interpolation. Instead we use a special adaptive interpolation technique. The idea of this method is to use available surface data to reproduce the geometry of geologic features, such as circular basins or linear mountain belts. In general, the crustal structure of such geologic features is measured in several places. For example, a number of seismic cross

sections depict the crustal structure of the ocean-continent transition. If neighboring sections are similar, we may assume that this structure is also similar within a local area. Thus, we use the known geometry of the continental margin as a guide to predict the structure in between the seismic lines. To avoid any bias in our processing of the gravity data we do not use the gravity field in constructing our crustal model.

[16] Previous analysis has shown that density anomalies in the upper crust may contribute significantly to the total crustal load (in addition to topography) and will have a correlation with the deep structure, such as Moho depth. For example, there is a clear inverse correlation between the thickness of low-density sedimentary basins and the thickness of the crystalline crust. The precise nature of such a correlation varies from region to region and depends on the density of the sediments within the basin [*Artemjev et al.*, 1994; *Lowry et al.*, 2000]. To incorporate all factors controlling near-surface load we define a parameter called the adjusted topography ( $T_{\text{adj}}$ ):

$$T_{\text{adj}} = T - H_{\text{sed}} \times [(\rho_{\text{crust}} - \rho_{\text{sed}})/\rho_{\text{crust}}] - B_{\text{water}} \times [(\rho_{\text{crust}} - \rho_{\text{w}})/\rho_{\text{crust}}], \quad (1)$$

where  $T$  is the actual topography (0 at sea level),  $H_{\text{sed}}$  is the thickness of the sediments within the basin,  $\rho_{\text{sed}}$  is the

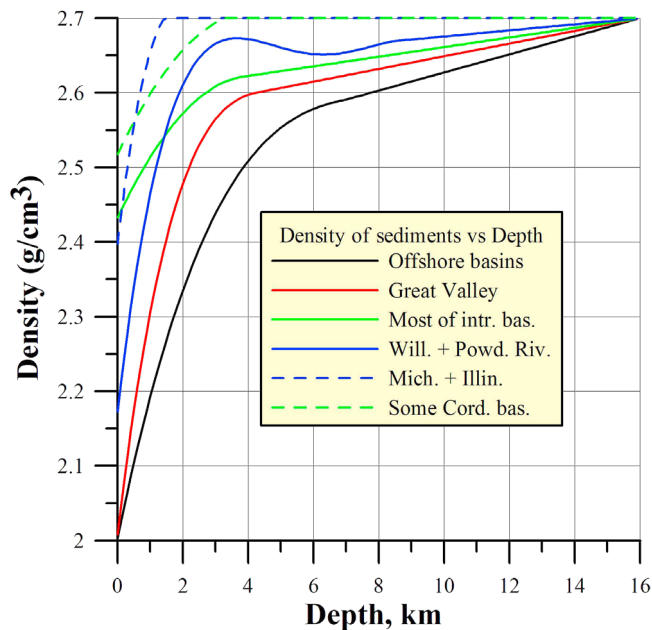


**Figure 5.** Density-depth curves for six typical geological provinces within North America. Density-depth relations were obtained from drill-hole logs for the upper 2–3 km and extended to greater depths using seismic data as a constraint. The lithology of the basin fill varies and is reflected in the highly variable density particularly above 6 km depth. At greater depths porosity is decreased and the sediments begin to lithify, converging toward an average density of 2.7 km/m<sup>3</sup>. These density-depth functions were used to calculate the gravitational attraction of the sediments in Figure 4.

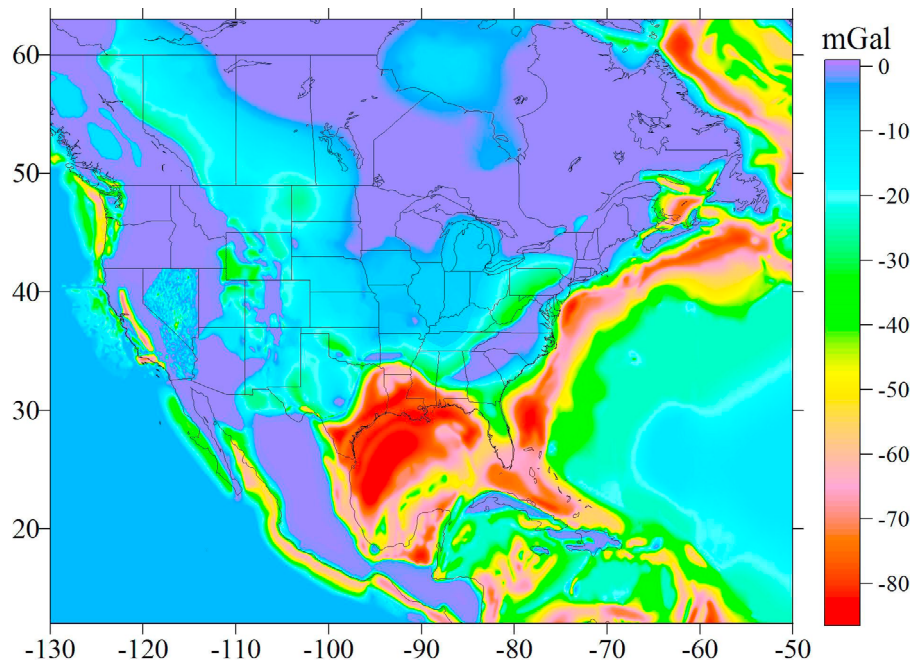


**Figure 6.** Gravitational effect of sediments relative to a sediment-free upper crust with an assumed density of  $2.7 \text{ g/cm}^3$ . Note that the gravitational correction for sediments is relatively small for nearly all of the continental interior, including regions that show strong anomalies in the mantle gravity field. This implies that the sediment correction cannot be responsible for these mantle gravity anomalies. The largest corrections, up to 80 mGal, are within the Gulf of Mexico and along the East Coast.

average density of the sediment column from the top to  $H_{\text{sed}}$ ,  $\rho_{\text{crust}}$  is the average density of the upper crust from the reference model,  $B_{\text{water}}$  is water depth in the sea areas, and  $\rho_w = 1030 \text{ kg/m}^3$  – water density.

[17] Thus the adjusted topography is obtained by numerical densification of water and sediments to be equal to the normal upper crust density (usually  $2670 \text{ kg/m}^3$ ) [Artemjev *et al.*, 1994]. After applying this transformation, a flat surface over any sedimentary basin is replaced by a depression that is proportional to the depth and average density of the basin. Using the topographic and sediment data already described, we compute the adjusted topography for the whole study area. We then compute the correlation coefficient between the adjusted topography and the Moho depth for all points where we have seismic data on crustal thickness. This analysis is performed in a sliding window with the radius of 200 km. This radius is increased if the number of points inside is low. If the correlation coefficient between these parameters is relatively high, we use regression coefficients we have obtained to define the Moho boundary in between the seismic determinations; otherwise we use standard interpolation. Following this procedure, we obtain a Moho map (Figure 7) that corresponds in all cases to the seismic determinations, but that also follows the geometry of the main tectonic provinces, as provided by the adjusted topography.

[18] After calculating the crustal thickness model, we need to estimate the density structure of the crust. Measured  $P$ -wave velocities within the crystalline crust were converted into densities using the equations provided by Christensen and Mooney [1995]. These density values have been interpolated onto the same standard grid used for the

thickness (i.e., layer depth) parameters used for the sediment and Moho models.

### 3. Gravity Effect of the Crust and Calculation of Mantle Gravity Anomalies

[19] We calculate the gravity effect of the density model of the crust relative to a horizontally homogeneous reference model. Our goal is to correct for the gravitational effect of the laterally varying crust by replacing it with the homogeneous reference crustal model. The mantle density is initially assumed to be constant and we obtain the residual or mantle gravity field, which reveals density variations in the mantle. The topography and bathymetry correction is already included in the Bouguer gravity calculation. Next, for each crustal layer we compute the difference between the actual crust and the reference crustal model (Figure 8). Thus, the crustal correction can be compared to a Bouguer correction that extends from the surface to the Moho. For example, the effect of low-density sediments is negative relative to the standard solid crust, and thus by removing this effect we increase the residual anomaly. Likewise, we account for density variations within the crystalline crust including variations in the crustal thickness (depth to Moho). Any uplift of the Moho boundary produces a positive gravity signal and leads to a reduction in the residual anomaly, whereas a deepening of the Moho produces a negative signal with an increase in the residual anomaly.

[20] It is generally assumed that any change in the horizontally homogeneous reference density model would lead only to a change in the reference level of the residual

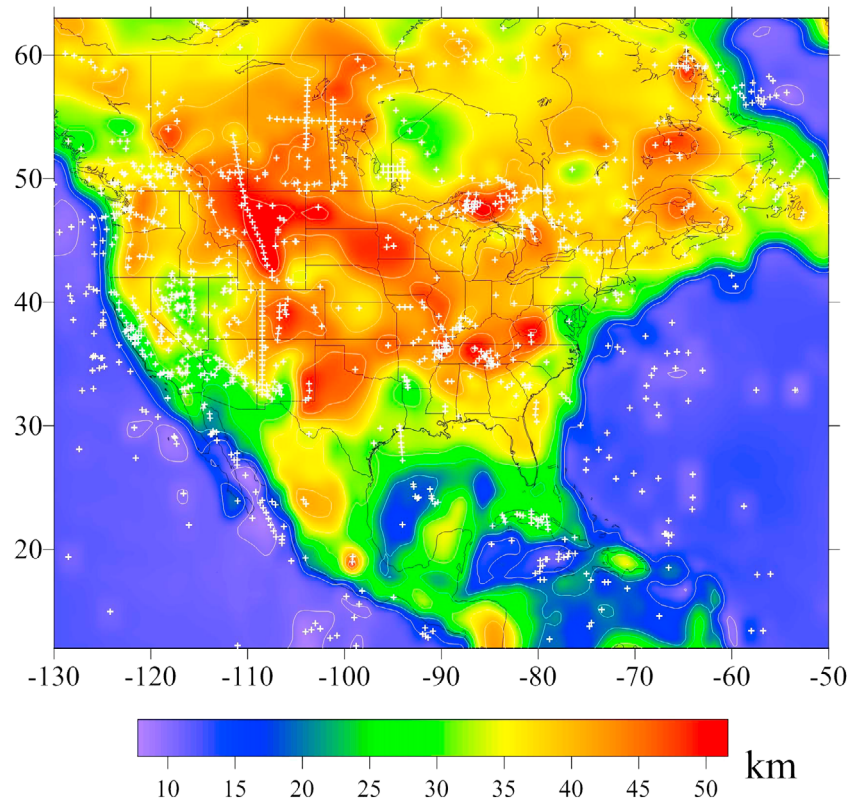


**Figure 7.** Depth of the crust-mantle boundary (Moho) below sea level. White crosses indicate data points where crustal thickness was determined mainly from active-source seismic profiles [Chulick and Mooney, 2002; additional subsequent profiles]. To obtain the mantle gravity structure, the measured crustal  $P$ -wave velocity structure was used to calculate the density structure of the crust needed to compute the gravitational effect (see text). Note that the crust has not been “removed”; rather, the lateral variations in the crust have been replaced by a uniform, 30 km thick homogeneous crust.

anomaly, since the effect of the layer with invariable density and boundaries is a constant value. However, this is completely true only if the average mantle density, which we attribute to the model, corresponds to the real one. We investigate possible uncertainties related to this factor later. For North America we apply the same reference density model of the lithosphere that was previously used in a global study [Kaban *et al.*, 2003]. This reference model corresponds to a continental crust with zero topography, a 15 km thick upper crust with a density of  $2.7 \text{ g/cm}^3$ , and a 25 km thick lower crust with a density of  $2.94 \text{ g/cm}^3$ . The average density of the uppermost mantle is set equal to  $3.35 \text{ g/cm}^3$ .

[21] The gravity anomaly of each layer within the Earth’s crust and mantle is calculated using a 3D algorithm for a spherical Earth, taking into account changes in density in the horizontal and vertical directions and the average elevation (or depth) of each cell. The sum of the gravity influence of each volume corresponding to the initial grids is computed in each grid cell on the surface. We use the algorithm of Artemjev and Kaban [1994], which is based on the formulas of Strakhov *et al.* [1989]. The estimated accuracy of the calculations is 1 mGal. We calculate the crustal gravity field for the area between  $32^\circ\text{N}$  latitude and  $63^\circ\text{N}$  latitude and between  $50^\circ\text{W}$  longitude and  $130^\circ\text{W}$  longitude. To account for density inhomogeneities outside our study

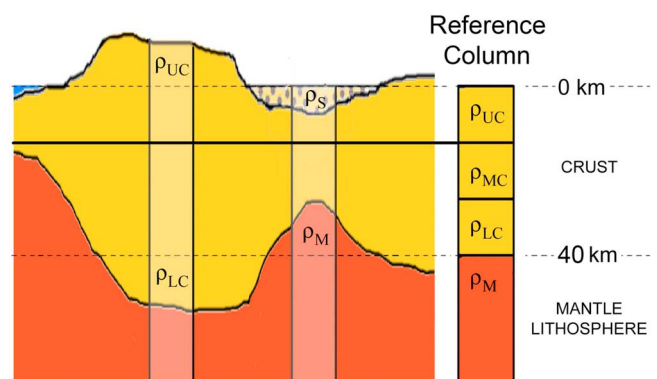


**Figure 8.** Illustration of (left) the laterally varying crust of North America and (right) the reference crustal column. To obtain the mantle gravity anomaly, a correction is applied to crustal columns on a dense grid covering all of North America. This eliminates the gravity effect of crustal density variations. The result is equivalent to the hypothetical situation whereby the North American crust is laterally homogeneous and, thus, contributes no gravity anomalies.

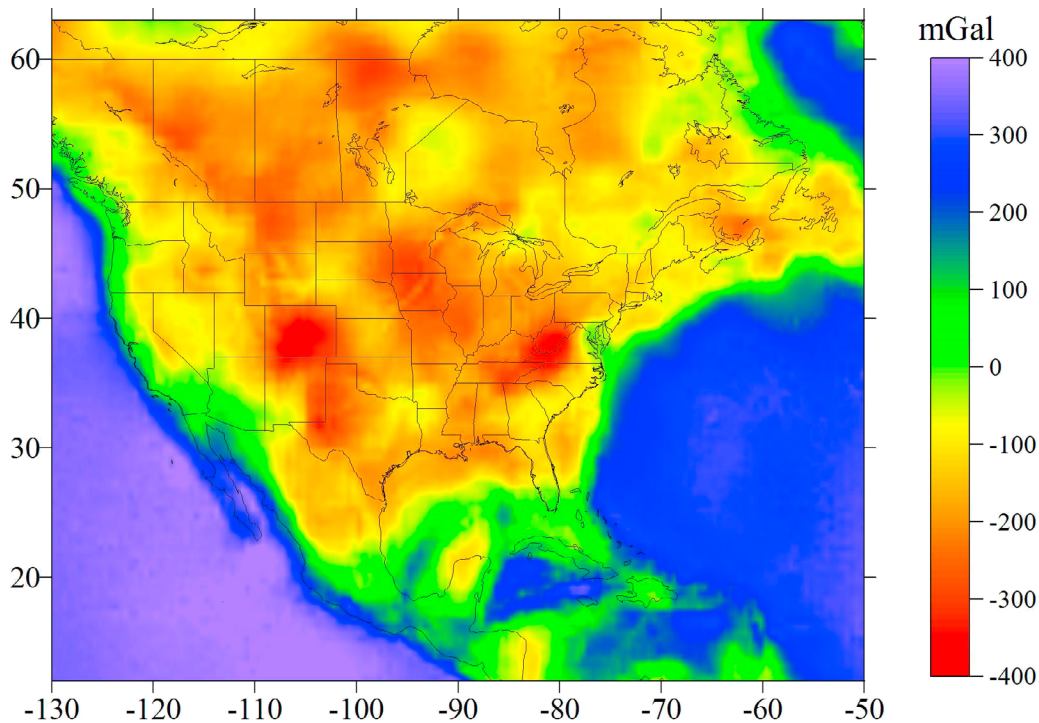


**Figure 9.** Crustal anomaly map. This map depicts the total correction that is applied to the Bouguer gravity data (Figure 3), excluding the correction for topography and bathymetry. The correction is positive in the ocean, and near-zero or negative for the continent, and reaches  $\pm 400$  mGal.

area we use crustal data from the global CRUST 2.0 model [Bassin *et al.*, 2000; Mooney *et al.*, 1998] as updated for several regions by Kaban *et al.* [2004]. Thus, the calculated field at each point reflects variations of the crustal layers over the entire Earth. Since these distant areas produce only a minor effect on the calculation, possible errors in this model are insignificant.

[22] The gravity effect of sediments relative to the normal upper crustal density is shown in Figure 6. This field varies from 0 to  $-85$  mGal. The most pronounced minima are located over the Gulf of Mexico and near the eastern continental margin. It is obvious that the correction for the density of sediments significantly changes the Bouguer gravity. In the same way we compute the effects of density variations within the crystalline crust and the effects of Moho depth variations. The total gravity effect of the crust excluding the topography/bathymetry correction, which is already removed from the Bouguer anomalies, is shown in Figure 9. The pattern of this crustal correction map may be compared with that of the initial Bouguer gravity (Figure 3). Although there are some similarities between these figures (negative anomalies over the continent and positive anomalies over the ocean), many important differences exist, especially when one compares the continental anomalies. The most striking feature is the absence of a pronounced difference between the eastern and the western parts of North America in the crustal gravity map, in contrast with the Bouguer gravity anomaly map. This difference implies that there are additional density inhomogeneities not incorporated in the initial model. Since the crustal density structure

is considered as known, the additional density variations are most likely located in the upper mantle.

[23] After removing the crustal correction from the Bouguer anomalies we obtain the mantle gravity anomalies (Figure 10). We set the mean value of this field to 0, since the absolute value depends on the choice of the reference model. Variations in the mantle gravity are as large as  $\pm 350$  mGal. The most pronounced minimum anomaly or density is found in the southwestern part of the United States, particularly in the Basin and Range province and the Gulf of California, while the densest lithosphere forms a complex distribution under Canada and the central and southeastern parts of the conterminous United States. We note that this mantle gravity anomaly map reflects lateral variations in both composition and temperature, both of which affect density. We now further process this map by applying a thermal correction for lateral variations in the mantle temperature to obtain the compositional mantle anomaly. These density variations might be located in the subcrustal layer of the lithosphere and/or below. In the present paper we do not attempt to distinguish these sources.

### 3.1. Uncertainties in the Mantle Gravity Anomalies

[24] It is essential to estimate uncertainties in the corrections that have been made to the gravity data to obtain the mantle anomaly map. Some aspects of this topic have been addressed with respect to global studies by Panasyuk and Hager [2000] and Kaban and Schwintzer [2001]. Here we consider the uncertainties for North America, which has much higher quality observed data compared to other

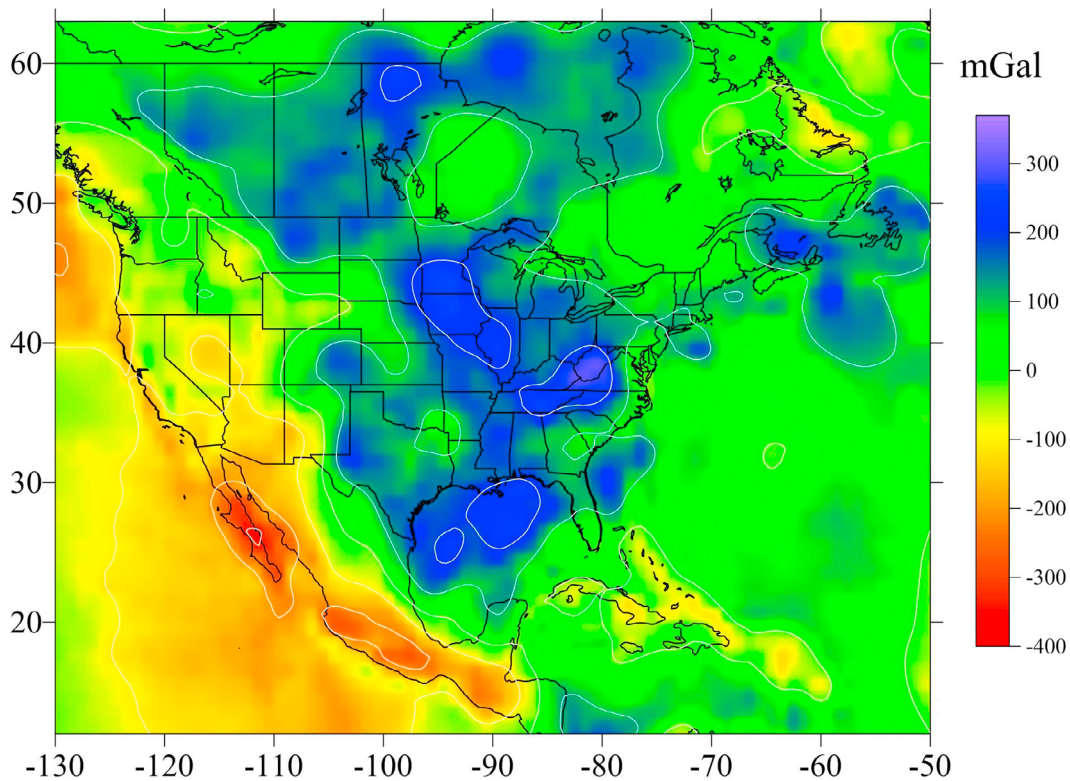


**Figure 10.** Mantle gravity anomaly map obtained by applying corrections for topography, sedimentary basins, and lateral variations in crustal structure. The hot, buoyant mantle in the southwestern United States and western Mexico shows strongly negative anomalies, whereas the colder mantle of the central and east portions of the study area shows either weakly positive (25–100 mGal) or strongly positive ( $\geq 100$  mGal) anomalies. The Atlantic Ocean has a near-zero anomaly, whereas the eastern Pacific Ocean shows a negative anomaly coincident with the East Pacific Rise. A pronounced positive anomaly coincides with Gulf of Mexico and several regions of the continental interior.

regions of the world. The following factors contribute to the overall error in the calculated mantle gravity anomalies: (a) the measured gravity and topography; (b) the crustal model, which includes the estimated thickness and density both of the sediments and of the solid crust; and (c) the assumed mean density of the upper mantle. Of these three factors we may ignore potential errors in the observed gravity and topography, since for North America these errors amount to only 1–2 mGal. However, the other two factors may contain substantial error. Active-source seismic refraction data provide the primary basis for the crustal model. A single seismic determination may contain substantial error. For example, the uncertainty in Moho depth could be up to 10% (4–5 km) for older (pre-1970s) seismic profiles. However, when we consider regions where several independent seismic studies have occurred, this uncertainty is significantly reduced. While constructing the crustal database for North America we have inspected all seismic models of the crust and removed questionable and/or inconsistent results from the analysis.

[25] As mentioned previously, sedimentary basins may contain thin high- or low-density layers, but in general smooth density-depth functions are adequate to describe each specific basin. Owing to compaction and metamorphism, the main density variations occur within the upper

6 km of the basin [e.g., *Beyer et al.*, 1985; *McCulloh*, 1967], and these depths are well documented by borehole and seismic data. Because of extensive hydrocarbon exploration, the thickness of sediments is known in even greater detail than is necessary for this study. Thus, following *Kaban et al.* [2002] and *Kaban and Schwintzer* [2001], we assume that the maximum error for the gravity effect of sediments at a medium ( $\geq 100$  km) to large ( $\geq 250$  km) scale (corresponding to approx. 180 and 70 spherical harmonic deg, respectively) is at most 15% or about 10–12 mGal for the deepest gravity minima (Figure 6).

[26] The error arising from the uncertainty in Moho depth can be estimated assuming a mean density contrast of  $0.35 \text{ g/cm}^3$  between the lower crust and the uppermost mantle. For a broad mantle gravity anomaly, which is based on many ( $>10$ ) seismic determinations from different seismic cross sections, the average regional depth to Moho is determined with an accuracy of about 2 km. This corresponds to a gravity error of about 30 mGal. In active tectonic regions and in areas with poor seismic coverage (with fewer than several determinations per anomaly), this uncertainty is doubled and may reach 60 mGal. This value corresponds to a depth-to-Moho accuracy of 10% ( $\sim 4$  km). In view of these considerations of uncertainty, we do not discuss mantle anomalies that are constrained by only one or two

**Table 2.** Potential Uncertainties of the Gravity Effect of the Crust, Temperature Variations in the Upper Mantle, and the Residual Gravity Field<sup>a</sup>

Source/ Type of Anomaly	Uncertainty
Sedimentary layer	Up to 15% or 10–12 mGal for thick sediments
Moho	30 to 60 mGal (good or moderate coverage of data)
Crystalline crust	25 to 50 mGal (for 20 to 40 km thick crust)
Total effect of crust and residual anomalies (RMS)	35 to 70 mGal
Gravity effect of temperature variations in mantle	50 to 70 mGal (corresponding to uncertainty of $\sim 100^\circ\text{C}$ for geothermal model [Goes and Van der Lee, 2002])
“Compositional” residual gravity anomalies (RMS)	60 to 100 mGal

<sup>a</sup>See text for detailed explanation.

measurements of crustal structure. The standard deviation in estimated crustal density is based on the uncertainty in the velocity-to-density formulas given by *Christensen and Mooney* [1995]. For each individual crustal layer this amounts to about  $\pm 0.05\text{ g/cm}^3$ . We expect that this uncertainty is reduced when we average the densities of several layers, as usually exist in seismic models of the crust. Assuming a typical three-layer model of the continental crust, the overall uncertainty of the solid crustal density is equal to approximately  $0.03\text{ g/cm}^3$ . Thus, the contribution of the crystalline crust to our error analysis depends on its thickness and may reach 25 to 50 mGal (for 20 to 40 km thick crust, respec-

tively). Note that a change in the assumed mean density of the mantle by  $0.03\text{ g/cm}^3$  yields an additional uncertainty in the calculated mantle gravity anomaly of 12 mGal.

[27] Uncertainties corresponding to different factors are summarized in Table 2. It should be noted that the relative weight of these factors depends on the data coverage and type of the crust. Usually these uncertainties do not correlate and thus the total uncertainty is much less than a sum of them. For example, the areas with a thick crust are usually characterized by an insignificant effect of sediments and by a stable, well-defined Moho. Therefore, we take into account the distribution of these uncertainties when estimating a cumulative error. Combining all error sources, the estimated standard deviation in the mantle gravity anomaly map varies from 35 mGal for the well-studied regions of North America with thin consolidated crust to about 70 mGal for the regions with thick crust and poor seismic coverage. In contrast, our residual mantle anomaly map shows a range of values as great as  $\pm 250\text{ mGal}$ , yielding a signal-to-noise ratio of at least 4 and frequently higher.

### 3.2. Mantle Gravity Anomalies Due to Temperature and Compositional Variations

[28] We find a large range of mantle gravity anomalies over North America (Figure 10). It is of interest to assess the origin of these mantle anomalies, that is, whether they are due to primarily temperature or compositional effects. Some indications for mantle temperatures may be obtained from seismic tomography data since *S*-wave velocity variations are chiefly controlled by temperature variations [*Röhm et al.*, 2000; *Goes and Van der Lee*, 2002]. In Figure 11 we show the *S*-wave velocity distribution at the depth of 100 km

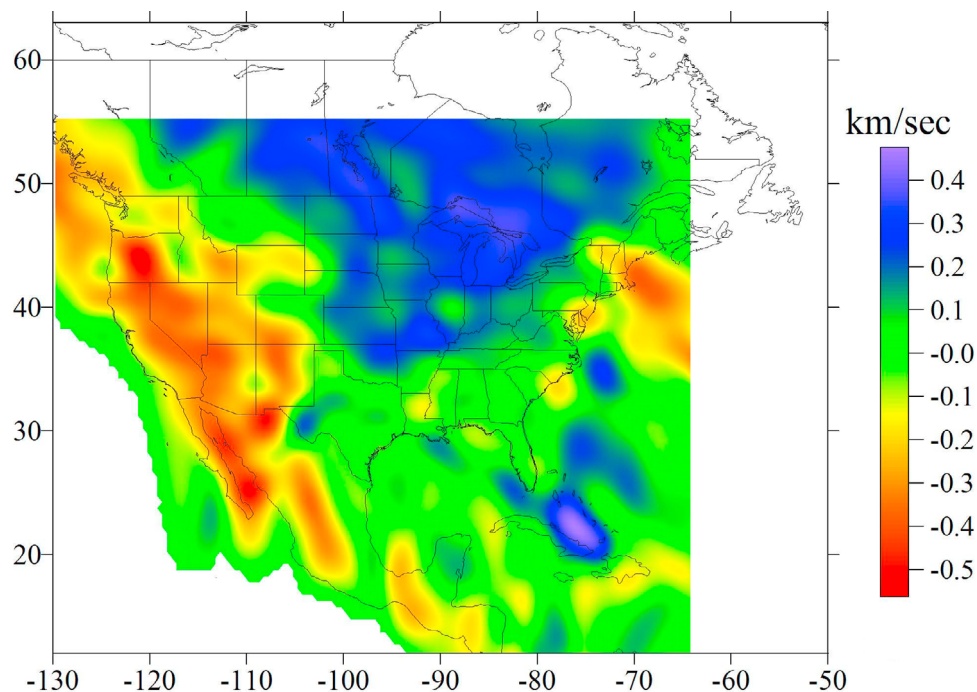


**Figure 11.** Seismic shear-wave anomaly map at a depth of 100 km determined from the inversion of Rayleigh wave phase velocities [*Van der Lee and Nolet*, 1997b]. Strong negative anomalies are found in the west (cf. Figure 10a) and strongly positive anomalies correlate with the Precambrian continental interior of Canada and the northern United States.

[*Van der Lee and Nolet, 1997b*]. Although we see some similarity between this map and the mantle gravity anomaly map (Figure 10), there are also substantial differences. The western part of the continental United States is characterized by a strong minimum in seismic velocities, which coincides with a corresponding minimum in the mantle gravity. However, in the central and eastern parts of North America the correlation between the two fields (Figures 10 and 11) is much weaker. The most prominent maximum for *S*-wave velocity is located under the Canadian Shield, where the mantle gravity is not at its strongest. Furthermore, the eastern and southeastern parts of the conterminous United States are characterized by strong positive mantle anomalies but have near-zero seismic velocity anomalies.

[29] To separate out the thermal compositional contributions to the mantle gravity map (Figure 10), we apply a complete upper mantle temperature correction, thereby isolating that portion of the mantle gravity that is due purely to composition. The thermal structure of the NA mantle was calculated by *Goes and Van der Lee [2002]* based on the *Van der Lee and Nolet [1997b]* seismic surface wave tomographic model. This seismic and temperature model extends to a depth of about 250 km with a depth resolution of about 50 km. The horizontal resolution approximately corresponds to the resolution of the residual mantle anomalies. The great advantage of using the seismic model of *Van der Lee and Nolet [1997b]* for mantle temperature estimations is that it was calculated using an a priori crustal model, thereby minimizing trade-offs between the velocity structure in the crust and the upper mantle. The crustal data used are the same that we used for the calculation of the mantle anomalies, which makes a comparison of these data sets consistent.

[30] *Goes and Van der Lee [2002]* present a detailed discussion of the assumptions underlying their conversion of *S*-wave velocity to temperature. The conversion is performed taking into account the possible existence of some melt fraction when the calculated temperature is close to solidus, as may be the case for the mantle beneath western North America. The authors have also considered the potential influence of compositional variations and provide an estimated accuracy of the conversion of *S*-wave velocity to temperature. Once they have estimated the mantle temperature, *Goes and Van der Lee [2002]* calculate variations in the mantle density distribution using published coefficients of thermal expansion. We use their temperature-derived density distribution to adjust our mantle gravity anomaly map (Figure 10). To avoid boundary effects outside North America we make use of the global upper mantle density model of *Kaban et al. [2003]*.

[31] After removing the temperature-induced gravity field from the mantle anomaly (Figure 10), we obtain a map of compositional mantle gravity anomalies (Figure 12). The amplitude of the gravity anomalies due to mantle temperature variations ranges from  $-150$  to  $+220$  mGal, which is about 50% of the amplitude of the total residual mantle anomaly shown in Figure 10. Figure 12 also contains some signal from below 275 km depth that was the limit of the temperature calculations. Density anomalies between 275 and 660 km deep may contribute to the gravity field in Figure 12, and these are discussed below in relation to the subducted Farallon slab [*Van der Lee and Nolet, 1997a*]. Density anomalies in the lower mantle will be relatively

weak with a long wavelength (i.e., spherical harmonics of order  $<12$  [*Forte and Perry, 2000*]) and thus will not be prominent in Figure 12.

### 3.3. Uncertainties in the Compositional Mantle Anomaly Map

[32] The temperature correction applied to the mantle anomaly map introduces additional uncertainties. These uncertainties are mostly due to the errors in the estimation of temperature based on seismic velocities. *Goes and Van der Lee [2002]* reported that the discrepancy between temperature estimates based on different seismic parameters (e.g., from *P*-wave velocity vs. *S*-wave velocity) usually does not exceed  $100^{\circ}\text{C}$ . The maximal gravity effect of such uncertainty could be up to 50–70 mGal (Table 2).

[33] The mantle temperature estimates of *Goes and Van der Lee [2002]* may be compared with the estimates obtained by other methods. *Artemieva and Mooney [2001]* estimated upper mantle temperatures for all continents (excluding Antarctica) from heat flow data. Their results, which have a lower resolution, are in good agreement with the average values of *Goes and Van der Lee [2002]*. We found that the difference between temperature-induced mantle gravity anomalies estimated from seismic vs. heat flow data is less than 50 mGal when we consider relatively large areas. This is consistent with our previously stated estimate of the uncertainty of the temperature correction.

[34] The total error in the calculation of the “compositional” residual anomalies may therefore reach 60–100 mGal, depending on the area. The amplitudes of the observed anomalies are significantly higher and reach  $\pm 250$  mGal (Figure 12). We have contoured the compositional anomaly map with a 100 mGal interval, thus emphasizing the largest anomalies that are well determined.

### 3.4. Interpretation of the Compositional Mantle Gravity Anomalies

[35] Western Canada and the United States have a near-zero compositional mantle anomaly (Figure 12; A), which indicates that the temperature correction has fully explained the uncorrected mantle anomaly (Figure 10). This supports the concept that the 1–2 km average topography of much of western North America is largely due to high temperatures in the uppermost mantle [*Hyndman and Lewis, 1999; Kaban and Mooney, 2001*]. This is also in agreement with geodynamic studies, which indicate that the dynamic effect of global mantle flow is insignificant with respect to the broad high topography of the western United States [*Perry et al., 2003*].

[36] The compositional mantle anomaly map clearly defines the depleted root of the Canadian shield (Figure 12; B). This strong ( $\geq 100$  MGal) negative compositional mantle anomaly is well known from previous geophysical and petrologic studies [*Jordan, 1978, 1981, 1988*] and may provide the buoyancy that has uplifted and exposed the Canadian shield. This result is in agreement with the results of *Perry et al. [2003]* and *Kaban et al. [2003]*. However, this new model provides more geographic detail compared to the previous studies; the depleted part of the sub-crustal lithosphere is localized and corresponds closely with the Canadian Shield rather than with major portions of central and north-eastern North America. Another strong negative composi-

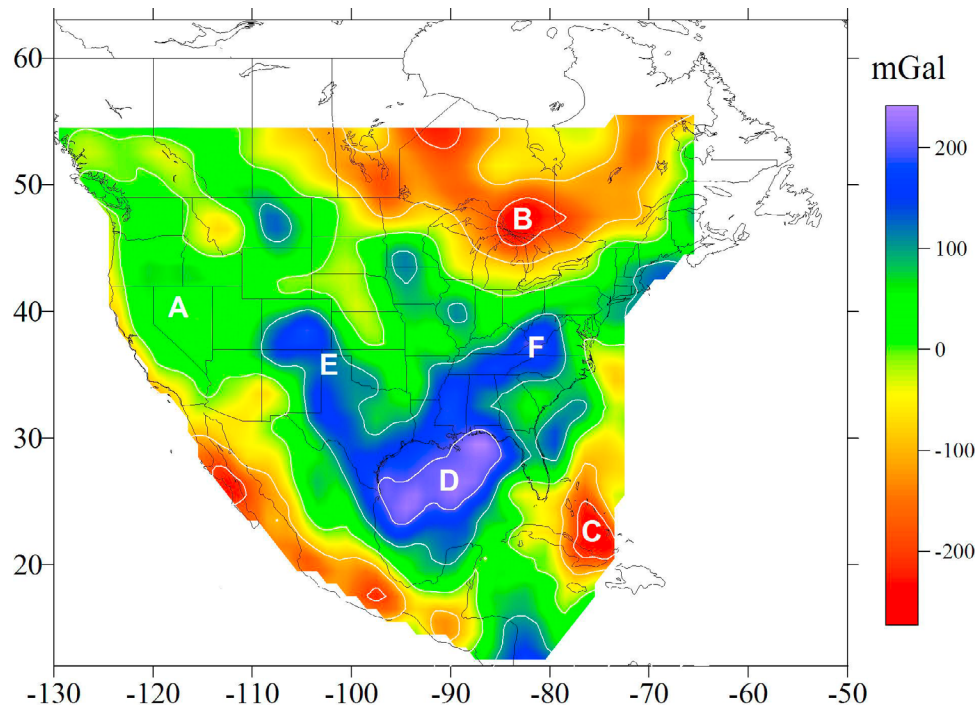


**Figure 12.** Compositional mantle gravity anomaly after removing the effect of thermal expansion due to lateral variations in mantle temperature. This map contains all corrections, topography, bathymetry, gravitational effects of sedimentary basins, and lateral variations within the crust (Figure 9), as well as a correction for the thermal state of the mantle, as inferred from seismic tomography (Figure 11). We identify six major features: (A) a near-zero anomaly in western North America, indicating that the high topography is supported by a positive thermal anomaly; (B) a depleted lithospheric root beneath the Canadian shield that is clearly evident; (C) a second region of mantle depletion correlated with the Bahamas; (D) a strong positive compositional anomaly beneath the Gulf of Mexico, perhaps due to eclogite in the uppermost mantle; (E) a NNW-trending anomaly on the SW edge of the North American craton that may be due to a lithospheric downwelling; (F) a NE-SW-trending positive anomaly located NW of the Grenville-Appalachian suture that may indicate a remnant slab fragment in the uppermost mantle. The overall picture is of a very compositionally heterogeneous uppermost mantle.

tional mantle anomaly is found north of Cuba (Figure 12; C) and may indicate a zone of depleted mantle, possibly a fragment of African lithosphere, beneath the shallow waters surrounding the Bahamas.

[37] The Gulf of Mexico displays the most positive ( $\geq 200$  mGal) compositional mantle anomaly (Figure 12; D). *Nettles and Dziewonski* [2008; Figure 15] report a positive  $S$ -velocity anomaly in the uppermost mantle coincident with this compositional mantle anomaly. Positive density anomaly D may contribute to the subsidence of the Gulf Coast, and we hypothesize that it is due to eclogite within the uppermost mantle.

[38] Anomaly E (Figure 12) trends NNW from Texas to Colorado and parallels the axis of the ancestral Rocky Mountains. What is remarkable about this anomaly is that it is perpendicular to the middle-to-late Proterozoic accretionary belts (Yavapai, Mazatzal, and Grenville provinces [Karlstrom *et al.*, 2001]) that form the southern margin of North America. This geometrical relation indicates that compositional mantle anomaly E postdates the Proterozoic accretion of these terrains. We consider two alternative models for the origin of the compositional mantle anomaly. *Hildebrand* [2009] proposes a model for the evolution of

the Cretaceous-Tertiary orogeny in the NA Cordillera that invokes westward-directed subduction (ca. 150–75 Ma) and slab breakoff (ca. 75 Ma). Compositional anomaly E correlates geographically with the hypothesized location of a slab remnant [Hildebrand, 2009] south of 40°N latitude. Alternatively, anomaly E may be the result of advection of the lithospheric mantle during a hypothesized period of eastward-directed, shallow, flat slab subduction [Bird, 1984, 1988]. Both of these models can explain our observed compositional mantle anomaly, but we prefer the advective downwelling model because the flat slab hypothesis appears to explain more completely the magmatic and tectonic events associated with the Laramide orogeny [Bird, 1984, 1988; Dickinson, 2004].

[39] Anomaly F (Figure 12) trends NE-SW and is located NW of the Grenville-Appalachian suture. This suggests an origin related to the closing of the paleo-Atlantic during the early stages of the Appalachian orogeny [Hatcher, 1989; Thomas, 1989]. Seismic tomography models for North America [e.g., *Nettles and Dziewonski*, 2008; *Bedle and Van der Lee*, 2009] report moderately high  $S$ -wave velocities in the uppermost mantle coincident with anomaly F at the SE margin of the craton. However, a distinct, isolated anomaly

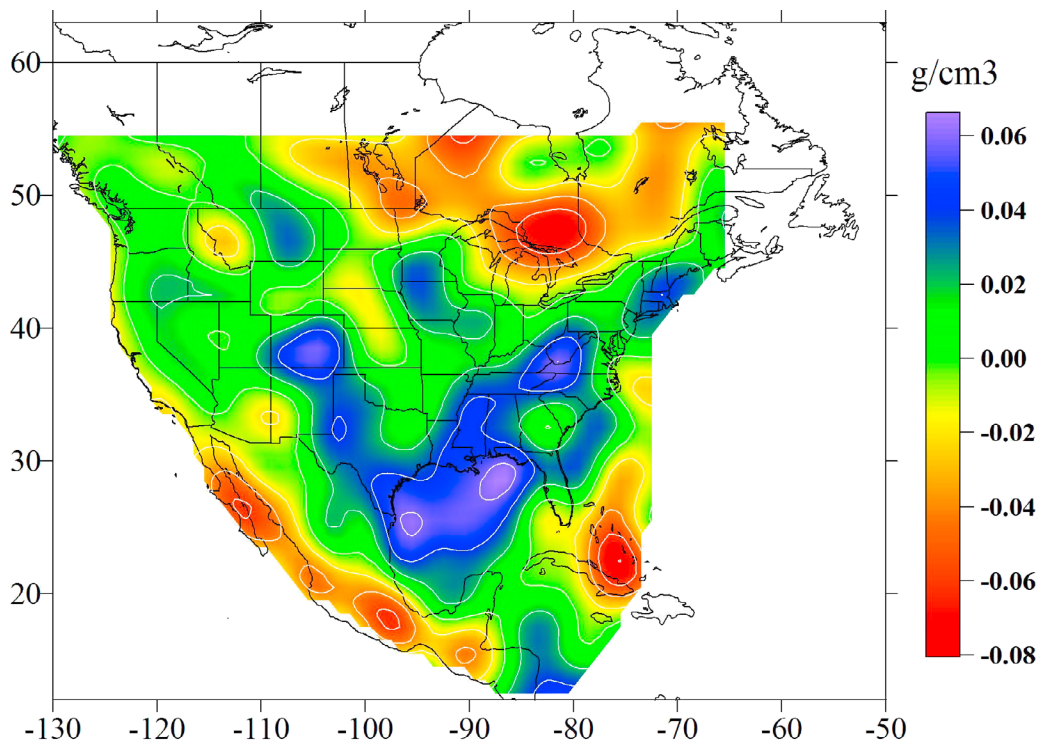


**Figure 13.** Upper mantle density anomalies calculated assuming that the causative anomalies are within the uppermost mantle in a 100 km thick layer (i.e., at an average depth of 40–140 km). This results in an estimated negative density anomaly of  $-0.03$  to  $-0.07$   $\text{kg/m}^3$  beneath the Canadian shield, a result that is consistent with lithospheric xenolith studies [Boyd, 1989]. The prominent positive density anomalies have a magnitude of  $+0.04$  to  $+0.06$   $\text{kg/m}^3$ , which may be explained by eclogite embedded in an upper mantle composed of peridotite [Boyd, 1989], but the uncertainty in the thickness of the anomalous layer precludes a definitive petrologic interpretation.

is not reported in seismic tomography models coincident with anomaly F [Grand, 1994; Grand et al., 1997; Van der Lee and Nolet, 1997b; Zhao, 2004; Zhou et al., 2006; Marone et al., 2007; Nettles and Dziewonski, 2008; Bedle and Van der Lee, 2009]. We note that this anomaly, like anomaly E terminates at  $40^\circ$  N latitude, whereas the Grenville-Appalachian suture continues to beyond  $50^\circ$  N. Anomalies D–F (Figure 12) provide evidence of significant compositional variations within the uppermost mantle of North America.

### 3.5. Quantitative Estimate of the Compositional Mantle Density Anomalies

[40] We use the compositional gravity anomalies (Figure 12) to estimate the magnitude of compositional density changes in the upper mantle under North America. Since the solution of the inverse gravity problem is generally not unique, we use a simple model that places all density variations within a 100 km thick layer. In the course of the inversion we suppress small-scale density variations (less than several hundred kilometers,  $>60$  spherical harmonic deg) that can be attributed to the previously discussed uncertainties in the crustal density and thermal models. The resulting compositional density distribution in the upper mantle is shown in Figure 13. The amplitude of the average density variations ranges from  $-0.07$  to  $+0.06$   $\text{g/cm}^3$ . The amplitude of these anomalies may be higher or lower, depending on the assumed layer thickness (here taken as 100 km), however,

the selection of a specific thickness should be based on some a priori knowledge. Given this uncertainty in the layer thickness, and hence the absolute density variations, specific petrologic interpretations, such as mantle metasomatism or the presence of eclogite, are poorly constrained.

### 3.6. Density Model for the Farallon Slab Beneath North America

[41] A portion of the mantle density anomalies identified in this study may be related to the presence of the subducted Farallon slab within the upper mantle [Bird, 1984, 1988]. Seismic tomography models have clearly shown a dipping high-velocity anomaly beneath eastern North America that has been postulated to be a remnant of the eastward-subduction Farallon slab [Grand, 1994; Grand et al., 1997; Van der Lee and Nolet, 1997a; Bijwaard et al., 1998; Zhao, 2004; Sigloch et al., 2008]. Part of this anomaly extends from the bottom of the mantle transition zone (660 km) to the midmantle (Figure 14, inset). We calculate the gravity expression of that portion of the Farallon slab below 660 km assuming a positive density contrast of  $0.025$   $\text{g/cm}^3$ . The resultant anomaly is in excellent geographic agreement with our anomaly D (Figure 12) located in the Gulf of Mexico. However, the D anomaly is in excess of 200 mGal, whereas the calculated Farallon slab anomaly is only 50 mGal. The amplitude of velocity perturbations might be significantly reduced by damping, which is an

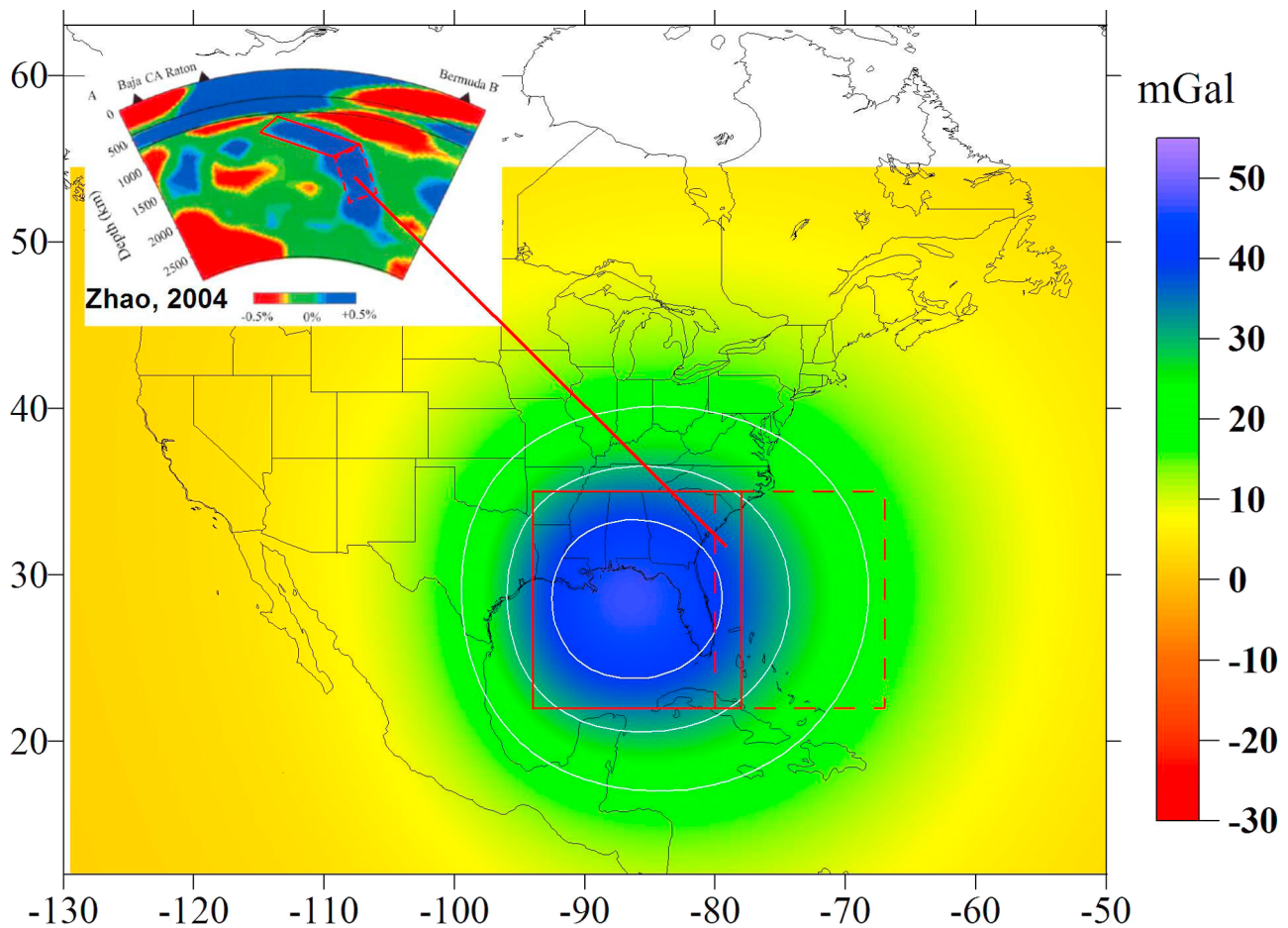


**Figure 14.** Gravity anomaly owing to the portion of the Farallon slab located below 660 km depth. Inset : seismic model of Zhao [2004]. This deep mantle density anomaly results in a gravity anomaly of 50 mGal and thus cannot explain the observed 200 mGal compositional anomaly labeled D in Figure 12. A shallower upper mantle density anomaly, such as an eclogite layer, is the favored interpretation for anomaly D.

essential part of any tomographic inversion. To estimate the upper bound of the possible gravity anomaly caused by the Farallon slab, we have used a maximal density contrast ( $0.025 \text{ g/cm}^3$ ) for the slab. We conclude that the portion of the Farallon slab below the mantle transition zone may contribute as much as 50 mGal to compositional gravity anomaly D (Figure 12) but the slab does not fully explain the entire 200 mGal anomaly.

[42] Van der Lee and Nolet [1997a] image fragments of the Farallon slab within the mantle transition zone. We have calculated the total effect of their seismic anomaly between 275 and 660 km (Figure 15). Three prominent positive anomalies are evident: (1) anomaly A still correlates with the cold root of the Canadian shield, (2) anomaly B correlates with the dense Juan de Fuca slab, and (3) anomaly C correlates with the shallow fragments of the Farallon slab and reaches a maximum magnitude of 60 mGal. Anomaly C (Figure 15) correlates with anomalies C and D of the compositional anomaly map (Figure 12) but, again, is significantly lower in magnitude (60 vs. 250 mGal). Although anomaly C (Figure 15) is wider than compositional anomaly D in Figure 12, this difference might be attributed to the

low resolution of the tomography model at greater depths. We note that the Gulf of Mexico anomalies calculated in Figures 14 and 15 sum to 100–120 mGal, which is about half of the anomaly we seek to explain (Figure 12). Thus, the influence of the Farallon slab appears to provide half of the compositional gravity anomaly in the Gulf of Mexico.

[43] The NE-SW-trending positive anomaly in the compositional gravity anomaly map (labeled E) and the NE-SW-trending anomaly F are too narrow to be explained by the Farallon slab as imaged by seismic tomography methods. For this reason our preferred model for anomaly E is a lithospheric drip, or advective downwelling, located at the western edge of the southern craton. Our preferred model for anomaly F is the presence of a fragment of a slab associated with the Appalachian orogeny.

#### 4. Evolution of the North American Upper Mantle

[44] The results presented here, combined with previous geologic and seismological investigations, provide insight

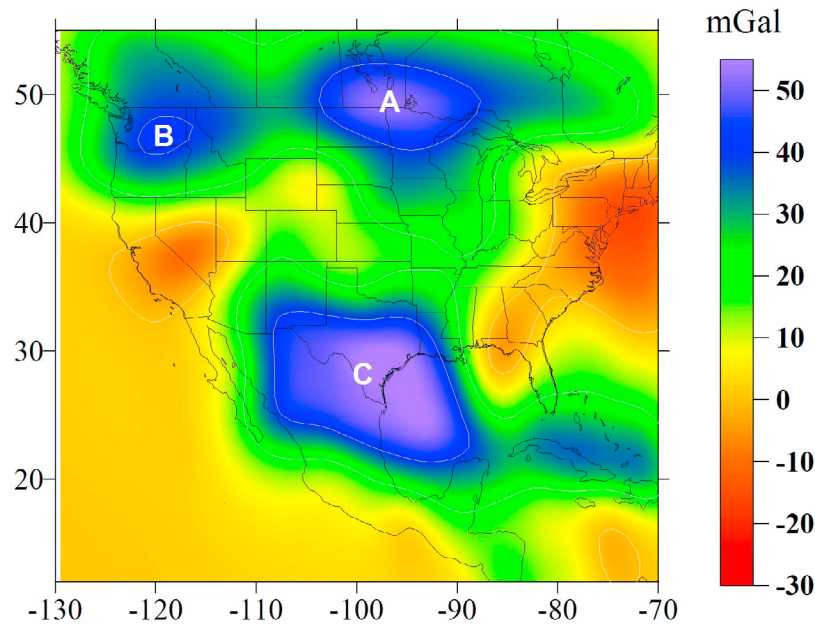


**Figure 15.** Gravity anomaly owing to the portion of the Farallon slab located above 660 km [Van der Lee and Nolet, 1997a]. Anomaly C has a magnitude of 50 mGal, too low to explain anomaly D in Figure 12.

**Figure 16.** Maps illustrating stabilization and growth of the North American continent. Inset (top left): lines A-A', B-B'-B'', and C-C' indicate cross sections locations that appear in Figure 17. Map A: Suture of the Wyoming, Trans-Hudson, Superior, and Slave/Roe/Hearne provinces occurred during the Trans-Hudson orogeny between 1.85 and 1.78 Ga, forming the cratonic core of Laurentia [Hoffman, 1988; Ross and Villeneuve, 2003]. The collision of these and other smaller Archean-early Proterozoic fragments created the core of the North American craton [Hoffman, 1988]. These events were preceded by the closing of Archean-aged ocean basins [Bleeker, 2003; Corrigan et al., 2005; Bleeker and Ernst, 2006]. Figure 17, cross sections 1 and 2, taken through line A-A', accompany this map view. Map B: Yavapai province was welded to the southeastern edge of the North American craton during the Yavapai orogeny (1.71–1.68 Ga). Yavapai province was formed from an assemblage of oceanic arc terranes 1.80–1.70 Ga. The Yavapai currently extends from present-day Arizona to Colorado (south of the Cheyenne belt) and northeast into the midcontinent [Van Schmus et al., 2007]. Map C: Mazatzal province, 1.68–1.60 Ga, accreted to the craton during the Mazatzal orogeny (1.71–1.62 Ga). Mazatzal province was formed from volcanic arcs at continental margins and backarcs. Mazatzal province includes volcanogenic greenstones composed of metamorphosed basalt, basaltic andesite, dacitic tuff, and rhyolite [Karlstrom et al., 2004; Whitmeyer and Karlstrom, 2007]. Granite-Rhyolite province accreted to the North American craton between 1.55 and 1.35 Ga. This province is composed primarily of A-type granites and anorthosites. Granite-Rhyolite province extends over a vast portion of the present-day United States and has a metamorphic overprint from the Grenville orogeny. Granite-Rhyolite province is largely concealed by the Paleozoic sedimentary cover of the midcontinent [Whitmeyer and Karlstrom, 2007]. Map D: The paleocontinent Laurentia formed through a series of continent-continent collisions, ultimately leading to the creation of the supercontinent Rodinia [Moores, 1991; Dalziel, 1991]. Grenville province collided with Granite-Rhyolite province along an eastward-directed subduction zone. The resulting Grenville orogeny caused a front of deformation that extends from the present-day southwestern United States through northeastern Canada. Grenville-aged deformation also extends into Granite-Rhyolite and Mazatzal provinces. Figure 17, cross section 3, taken through line B-B'-B'', accompanies this map view. Map E: Rifting was initiated along the midcontinent rift, located in the south-central area of Superior province and extending southward through the Yavapai and northern Mazatzal provinces. Rifting was aborted, and mantle-derived basalts filled the midcontinent rift graben. The core of North America remained intact, with a new series of resultant faults passing through the center of the continent. Rodinia broke apart along the western edge of Laurentia between 0.78 and 0.68 Ga [Dalziel, 1991; Moores, 1991; Karlstrom et al., 1999; Li et al., 2008]. This successful rifting opened the Pacific Ocean. Later, rifting along the eastern margin (0.6 Ga) created the paleo-Atlantic Ocean. Figure 17, cross section 4, taken through line C-C', accompanies this map view. Map F: Closing of the paleo-Atlantic in the Paleozoic created the Appalachian province as Africa collided with the east coast of Laurentia, suturing a host of schistose rocks to present-day eastern United States and Canada. Appalachian province and smaller subterranean subducted beneath Grenville and Granite-Rhyolite province sequences. Basement rocks of present-day eastern United States were thus accreted during the Appalachian orogeny. Figure 17, cross section 5, taken through line C-C', accompanies this map view. Map G: Cordilleran province was accreted and deformed along the western margin of the North American craton. The modern Atlantic Ocean was created by the rifting of the eastern margin of North America. Figure 17, cross section 6, taken through line C-C', accompanies this map view sequence.

into how the upper mantle beneath North America has evolved. As already mentioned, in the present study we have not attempted to distinguish lithospheric versus sublithospheric contributions to the total mantle anomaly. However, we may assume that a major part of the composition density variations should be located within the geologically more complex lithosphere. Otherwise, it is unlikely that these anomalies could be preserved for a relatively long period of time. Our mantle compositional anomaly map (Figure 12) clearly outlines the depleted tectosphere beneath the Archean

Canadian shield. In contrast, depleted mantle is not found beneath the U.S. portion of the NA craton, where much of the cratonic mantle shows a near-zero density anomaly (Figure 12). Positive density anomalies, D–F (Figure 12), appear to correlate with (1) the anomalous upper mantle beneath the Gulf of Mexico (D), (2) a lithospheric advective downwelling located at the SW edge of the Proterozoic craton (E), and (3) a fragment of subducted lithosphere associated with the Appalachian orogeny (F). We illustrate the processes that have formed and modified the litho-

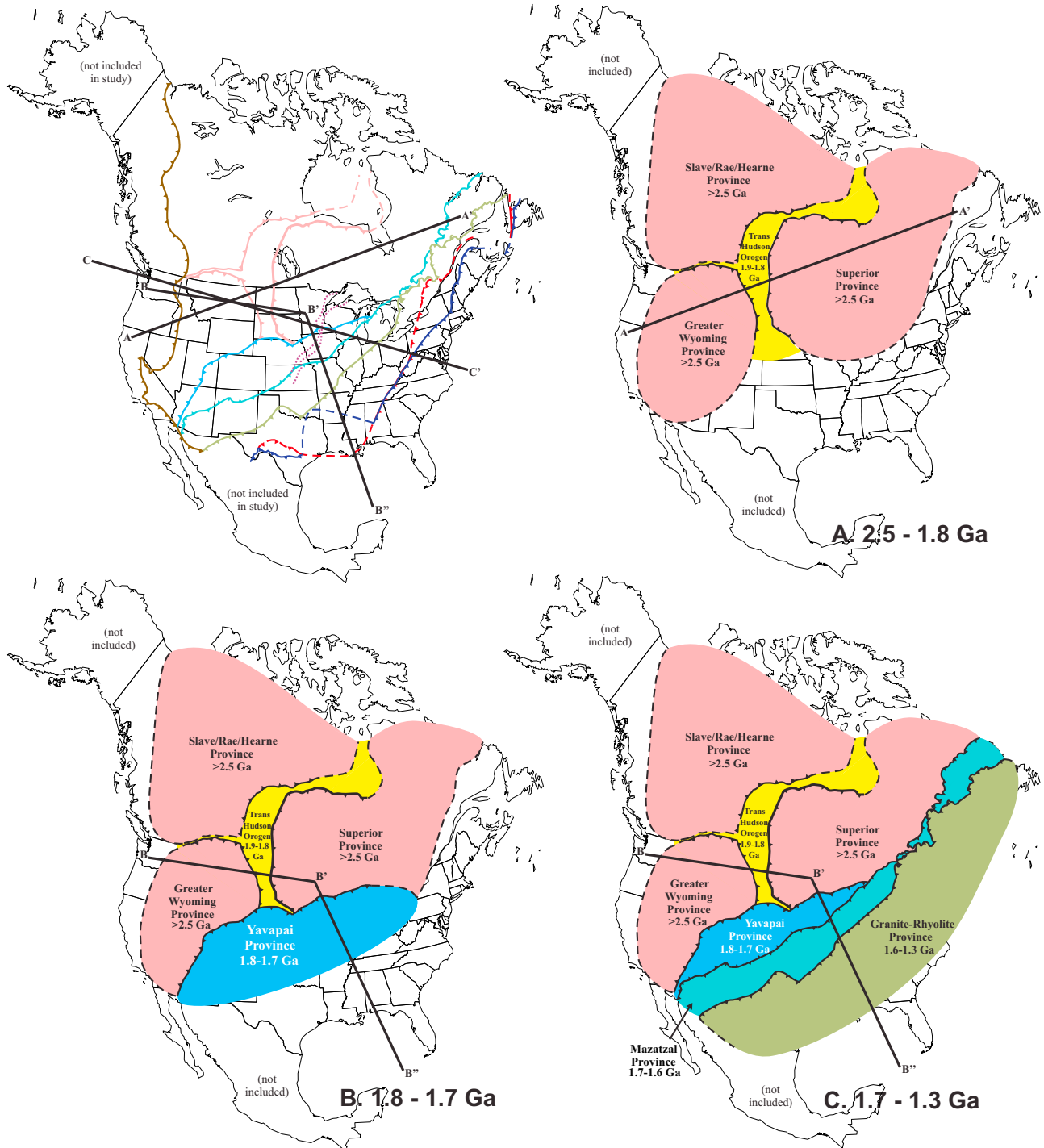


Figure 16

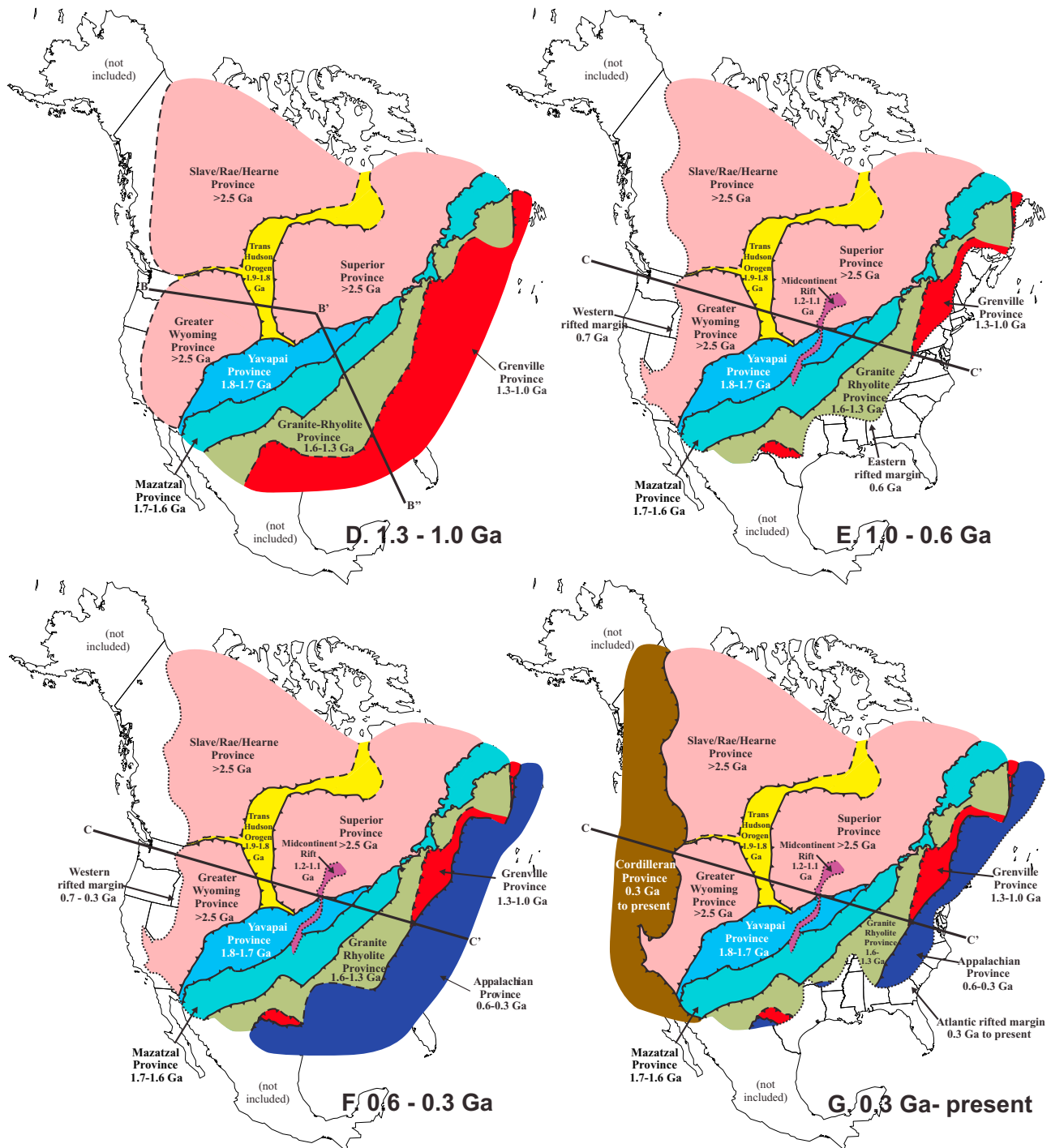


Figure 16. (continued)

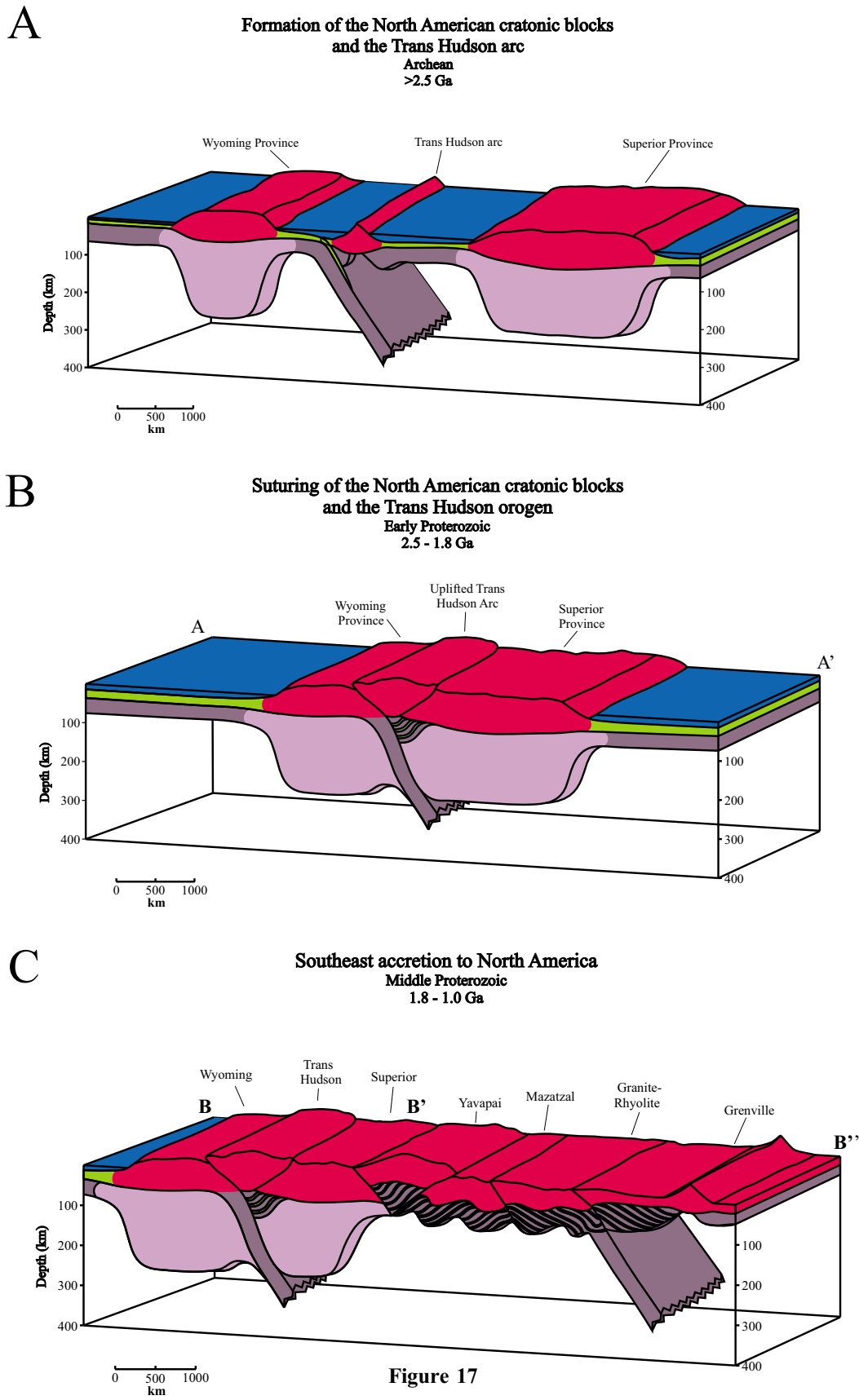


Figure 17

sphere of NA in map view (Figure 16) and in cross sections (Figure 17). In map view (Figure 16) the growth of the NA continent is characterized by stabilization of the Archean/early Proterozoic core (Figure 16a). During the Proterozoic a series of exotic terrains accretes to the SW margin (Figures 16b–16d), followed by rifting to form the proto-Atlantic (Figure 16e). The Appalachian orogeny (450–350 Ma; Figure 16f) is followed by the rifting and opening of the modern Atlantic Ocean on the east coast and the accretion and deformation of the Western Cordillera on the west coast (Figure 16g).

[45] We illustrate the evolution of the mantle lithosphere in six simplified cross sections (Figure 17). These cross sections illustrate the complex evolution of the subcrustal lithosphere over the past 2.5 Ga and depict the diversity of processes that have acted to form the NA upper mantle. These processes are documented in our analysis of the NA gravity data, including continental extension (Figure 12; A), the stabilization of the Archean craton (Figure 12; B), regions of mantle depletion of uncertain provenance (Figure 12; C), dynamic subsidence (Figure 12; D), advective instabilities (Figures 12 and 17; E, cross section 6), and paleoplate subduction (Figures 12 and 17; F, cross section 6). The broad-scale geologic complexity of the mantle lithosphere is therefore comparable to the geological complexity of the continental crust.

## 5. Conclusions

[46] We find that crustal density variations within sedimentary basins and the crystalline crust are compensated in

the uppermost mantle. Crustal corrections applied to NA Bouguer gravity data reveal significant upper mantle density anomalies that are of thermal and compositional origin. Maxima and minima in mantle gravity anomalies impose stresses on the base of the crust and these correlate with loci of crustal seismicity (Figure 10b). This process is similar to seismicity induced by vertical buoyancy forces associated with glacial rebound.

[47] To separate thermal anomalies from compositional anomalies, we apply a thermal correction to the mantle anomaly map (Figure 10a) to obtain the mantle compositional anomaly map (Figure 12). We find that (a) the mantle lithosphere beneath the Canadian shield has a pronounced low-density anomaly that has a compositional origin (depletion), as found in previous studies; (b) the low-density mantle anomaly beneath western North America is well modeled by a purely thermal correction; (c) there is a region of low-density (depleted?) uppermost mantle beneath the greater Bahamas region; (d) the Gulf of Mexico is underlain by a pronounced positive compositional anomaly that may contribute to the subsidence of the Gulf; (e) a linear positive compositional anomaly at the southwestern edge of the craton may be an advective downwelling that has not been identified previously; and (f) a linear positive compositional anomaly coinciding with the NW edge of the Grenville-Appalachian suture (south of 40°N) may be caused by a stalled slab that has not previously been identified.

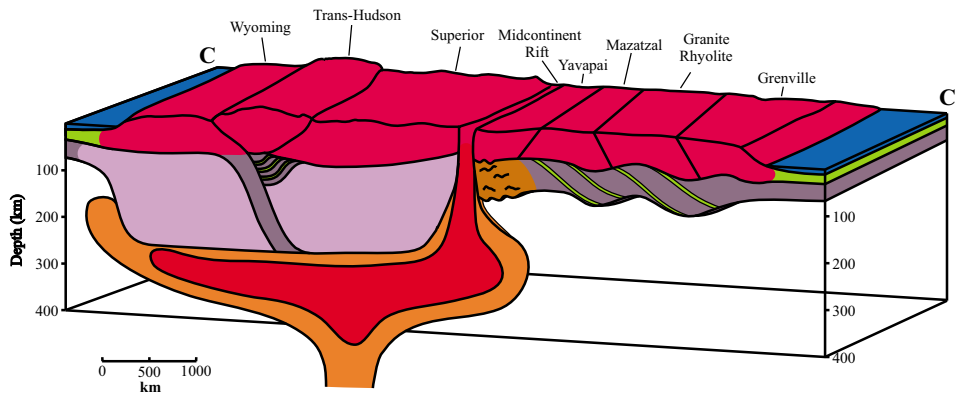
[48] Our study fills in several details concerning the 3D structure of the NA upper mantle. We use these insights to construct a concise outline of the evolution of the mantle lithosphere depicted in cross-sectional view. We find that

---

**Figure 17.** Cross sections illustrating main events in the formation of the lithospheric mantle beneath the North America continent. These cross sections are simplified to highlight the principal geological processes that have formed and modified the mantle lithosphere over the past 2.5 Ga. Cross section A: During the early Proterozoic, the Archean Wyoming and Superior provinces collided and the Wyoming oceanic lithosphere subducted beneath the Superior. Resulting subduction-related volcanism formed the Trans-Hudson volcanic arc. This cross section is the precursor to map view A in Figure 16. Cross section B: Trans-Hudson orogen occurred between 1.85 and 1.78 Ga, accreting the Wyoming and Superior cratons along with the Trans-Hudson volcanic arc into the cratonic core of Laurentia [Hoffman, 1988; Ross and Villeneuve, 2003]. Trans-Hudson belt includes Archean fragments, reworked Archean crust, and juvenile arcs along a zone that extends from present-day Montana to Hudson Bay [Whitmeyer and Karlstrom, 2007]. This cross section matches map A in Figure 16. Cross section C: The Yavapai orogeny (1.71–1.68 Ga) brought the Yavapai province to the North American craton. Mazatzal and Granite-Rhyolite provinces collided with the eastern edge of Laurentia and adhered between 1.68 and 1.35 Ga. The addition of the Grenville province to the eastern portion of Laurentia formed the supercontinent Rodinia at 1.1 Ga [Karlstrom and Whitmeyer, 2007]. This cross section accompanies map D in Figure 16. Cross section D: Rifted occurred in the mid-continent between the boundaries of the Superior and Yavapai provinces as shown in the center of this diagram. The craton formed by Wyoming, Trans-Hudson, and Superior provinces partially rifted away from that of the eastern provinces (northeastern Yavapai, Mazatzal, Granite-Rhyolite, and Grenville). This cross section accompanies map E in Figure 16. Farther to the west (not depicted here), Rodinia was rifted, leading to the separation of Laurentia and the western continents (Australia, etc.), opening a paleo-Pacific ocean. Cross section E: The Appalachian orogeny occurred with the closing of the paleo-Atlantic, deforming and thickening the mantle lithosphere beneath the Grenville and Granite-Rhyolite provinces. Slab breakoff left a fragment of the westward-directed subduction zone in the uppermost mantle beneath the eastern Grenville province, here hypothesized to account for mantle anomaly F (Figure 12). This cross section corresponds to map F in Figure 16. Cross section F: Subduction of the Pacific plate as initiated beneath the west coast of North America. A continental magmatic arc extends along the west coast, and the western cordillera is formed during a period of eastward-directed flat slab subduction that created lithospheric mantle anomaly E. Slab rollback and crustal extension in the Basin and Range province created space for asthenospheric upwelling and the creation of mantle anomaly A (Figure 12). Rifting occurs along the east coast forming the Atlantic Ocean. The mantle lithosphere preserves a >2.5 Ga history of continental growth, including subduction, rifting, and deformation. As is evident in the cross section, the broad-scale geologic complexity of the subcrustal mantle lithosphere beneath North America is as complex as that of the crust.

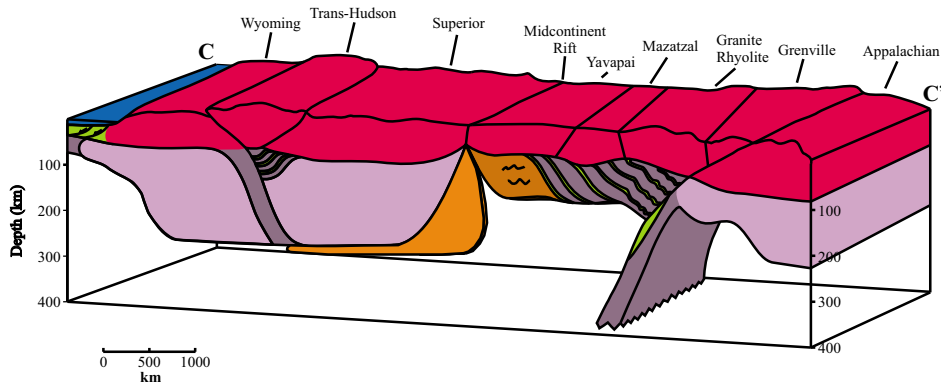
D

**Rifting of North America**  
Late Proterozoic  
1.0 - 0.6 Ga



E

**Appalachian accretion to North America**  
Phanerozoic  
0.6 - 0.3 Ga



F

**Cordilleran Tectonics and East Coast Rifting**  
Phanerozoic  
0.3 Ga - present

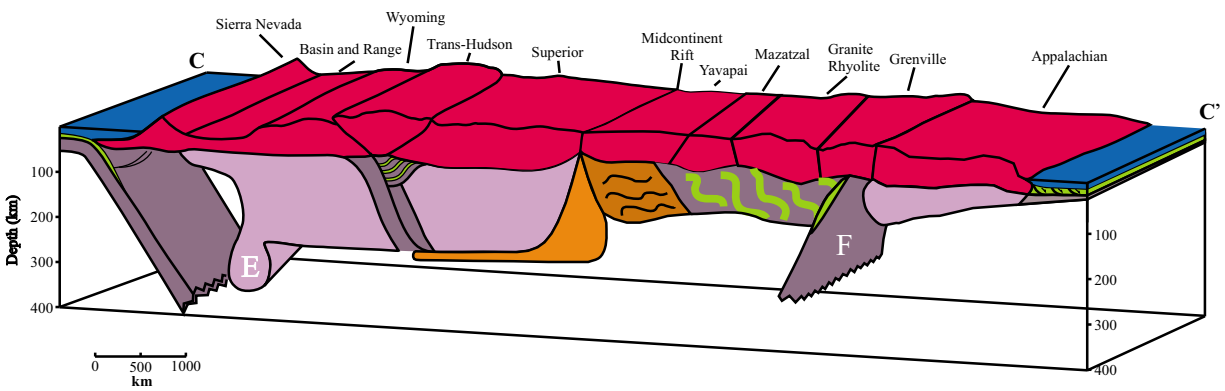


Figure 17. (continued)

the mantle contains far more structural complexity, as evidenced by the density structure, than has previously been documented.

[49] **Acknowledgments.** We gratefully acknowledge the support of the USGS Earthquake Hazards Program, part of the National Earthquake Hazards Reduction Program (NEHRP) and the German Geosciences Research Center (GFZ), Potsdam, and German Research Society grantRO-2330/4-1/2. This paper has been improved by review comments provided by F. Pollitz, S. Detweiler, G. S. Chulick, and journal editor R. Nowack, as well as two anonymous reviewers.

## References

- Artemieva, I. M., and W. D. Mooney (2001), Thermal thickness and evolution of Precambrian lithosphere: A global study, *J. Geophys. Res.*, *106*, 16,387–16,414, doi:10.1029/2000JB900439.
- Artemjev, M. E., and M. K. Kaban (1986), The free mantle surface—new possibilities to reveal subcrustal inhomogeneities from the structure of the Earth crust, *J. Geodynam.*, *5*, 25–44.
- Artemjev, M. E., and M. K. Kaban (1994), Density inhomogeneities, isostasy and flexural rigidity of the lithosphere in the Transcaspien region, *Tectonophysics*, *240*, 281–297.
- Artemjev, M. E., M. K. Kaban, V. A. Kucherinenko, G. V. Demjanov, and V. A. Taranov (1994), Subcrustal density inhomogeneities of northern Eurasia as derived from the gravity data and isostatic models of the lithosphere, *Tectonophysics*, *240*, 248–280.
- Bassin, C., G. Laske, and G. Masters (2000), The current limits of resolution for surface wave tomography in North America, *Eos Trans. AGU*, *81*, F897.
- Bedle, H., and S. Van der Lee (2009), *S* velocity variation beneath North America, *J. Geophys. Res.*, *114*, B07308, doi:10.1029/2008JB005949.
- Beyer, L. A., S. L. Robbins, and F. G. Clutson (1985), Basic data and preliminary density and porosity profiles for twelve borehole gravity surveys made in the Los Angeles, San Joaquin, Santa Maria and Ventura Basins, California, 67 pp., U.S. Geological Survey Open File Report, 85–42.
- Bijwaard, H., W. Spakman, and E. Engdahl (1998), Closing the gap between regional and global travel time tomography, *J. Geophys. Res.*, *103*(B12), 30,055–30,078, doi:10.1029/98JB02467.
- Bird, P. (1984), Laramide crustal thickening event in the Rock Mountain foreland and Great Plains, *Tectonics*, *3*(7), 741–758, doi:10.1029/TC003i007p00741.
- Bird, P. (1988), Formation of the Rocky Mountains, western United States: A continuum computer model, *Science*, *239*, 1501–1507, doi:10.1126/science.239.4847.1501.
- Bleeker, W. (2003), The late Archean record: A puzzle in ca. 35 pieces; *Lithos*, *71*, 99–134.
- Bleeker, W., and R. Ernst (2006), Short-lived mantle generated magmatic events and their dyke swarms: The key to unlocking Earth's paleogeographic record back to 2.6 Ga, in *Dyke Swarms—Time Markers of Crustal Evolution*, edited by E. Hanskiet et al., pp. 3–26, A. A. Balkema, Rotterdam.
- Bostock, M. G. (1997), Anisotropic upper-mantle stratigraphy and architecture of the Slave craton, *Nature*, *390*, 329–395, doi:1038/37102.
- Boyd, F. R. (1989), Compositional distinction between oceanic and cratonic lithosphere, *Earth Planet. Sci. Lett.*, *96*, 15–26.
- Burchfiel, B. C., D. S. Cowan, and G. A. Davis (1992), Tectonic overview of the Cordilleran orogen in the western U.S., in *The Cordilleran Orogen: Conterminous U.S.*, edited by B. C. Burchfiel, P. W. Lipman, and M. L. Zoback, vol. G-3, pp. 407–480, Geological Society of America, Geology of North America, Boulder, Colo.
- Burdick, L. J., and D. V. Helmberger (1978), The upper mantle *P*-velocity structure of the western United States, *J. Geophys. Res.*, *83*(B4), 1699–1712, doi:10.1029/JB083iB04p01699.
- Christensen, N. I., and W. D. Mooney (1995), Seismic velocity structure and composition of the continental crust: A global view, *J. Geophys. Res.*, *100*(B6), 9761–9788, doi:10.1029/95JB00259.
- Christiansen, R. L., and P. W. Lipman (1972), Cenozoic volcanism and plate-tectonic evolution of the western United States: 1, Early and middle Cenozoic, *Philos. Trans. R. Soc. London, Ser. A*, *271*, 217–248.
- Chulick, G. S., and W. D. Mooney (2002), Crustal structure of North America and adjacent oceanic basins: A synthesis, *Bull. Seis. Soc. Am.*, *92*, 2478–2492.
- Corrigan, D., Z. Hajnal, B. Nemeth, and S. B. Lucas (2005), Tectonic framework of a Paleoproterozoic arc-continent to continent-continent collisional zone, Trans-Hudson Orogen, from geological and seismic reflection studies, *Can. J. Earth Sci.*, *42*, 421–434.
- Cook, F. A., A. J. van der Velder, K. W. Hall, and B. J. Roberts (1999), Frozen subduction in Canada's Northwest Territories: Lithoprobe deep lithospheric reflection profiling of the western Canadian Shield, *Tectonics*, *18*(1), 1–24, doi:10.1029/1998TC900016.
- Dalziel, I. W. D. (1991), Pacific margins of Laurentia and East-Antarctica—Australia as a conjugate rift pair: Evidence and implications for an Eocambrian supercontinent, *Geology*, *19*, 598–601.
- Dickinson, W. R. (2004), Evolution of the North American Cordillera, *Annu. Rev. Earth Planet. Sci.*, *32*, 13–45, doi:10.1146/annurev.earth.32.101802.120257.
- Dickinson, W. R., and W. S. Snyder (1978), Plate tectonics of the Laramide orogeny, in *Cenozoic Tectonics and Regional Geophysics of the Western Cordillera, Geological Society of America Memoir 152*, edited by R. B. Smith and G. P. Eaton, pp. 335–366, Geol. Soc. Am., Boulder, Colo.
- Dorman, J. (1969), Seismic surface-wave data on the upper mantle, in *The Earth's Crust and Upper Mantle, AGU Geophys. Monogr. Ser.*, vol. 13, edited by P. J. Hart, pp. 257–265, AGU, Washington, D. C.
- Dorman, L. M., and B. T. R. Lewis (1970a), Experimental isostasy: 1. Theory of determination of the Earth's isostatic response to a concentrated load, *J. Geophys. Res.*, *75*(17), 3357–3365, doi:10.1029/JB075i017p03357.
- Dorman, L. M., and B. T. R. Lewis (1970b), Experimental isostasy: 2. An isostatic model for the USA derived from gravity and topographic data, *J. Geophys. Res.*, *75*(17), 3367–3386, doi:10.1029/JB075i017p03367.
- Dorman, L. M., and B. T. R. Lewis (1972), Experimental isostasy: 3. Inversion of the isostatic Green function and lateral density changes, *J. Geophys. Res.*, *77*(17), 3068–3077, doi:10.1029/JB077i017p03068.
- E Exxon (1985), *Tectonic Map of the World*, Am. Assoc. Petrol. Geol., Tulsa, Okla.
- Frezzon, S. I., T. M. Finn, and J. H. Lister (1983), Total thickness of sedimentary rocks in the conterminous United States, *U.S. Geological Survey Open File Report*, 83–920, U.S. Geological Survey, Boulder, Colo.
- Fuis, G., T. Ryberg, N. Godfrey, D. Okaya, and J. Murphy (2001), Crustal Structure and tectonics from the Los Angeles basin to the Mojave Desert, southern California, *Geology*, *29*, p. 15–18.
- Gardner, J. V., D. A. Cacchione, D. E. Drake, B. D. Edwards, M. E. Field, M. A. Hampton, H. A. Karl, N. H. Kenyon, D. G. Masson, D. S. McCulloch, and M. S. Grim (1992), Maps showing sediment isopachs in the deep-sea basins of the Pacific continental margin, scale 1:1,000,000, Miscellaneous investigations series, *Maps I-2089-A, I-2090-A, I-2091-A*, U.S. Geological Survey, Boulder, Colo.
- Godey, S., R. Sneider, A. Villasenor, and H. Benz (2003), Surface wave tomography of North America and the Caribbean using global and regional broadband networks: Phase velocity maps and limitations of ray theory, *Geophys. J. Int.*, *152*(3), 629–623.
- Godson, R. H. (1985), Preparation of a digital grid of gravity anomaly values of the conterminous United States, in *The Utility of Regional Gravity and Magnetic Anomaly Maps*, edited by W. J. Hinze, pp. 38–45, Soc. Explor. Geophys., Tulsa, Okla.
- Goes, S., and S. Van der Lee (2002), Thermal structure of the North American uppermost mantle inferred from seismic tomography, *J. Geophys. Res.*, *107*(B3), 2050, doi:10.1029/2000JB000049.
- Grand, S. (1994), Mantle shear structure beneath the Americas and surrounding oceans, *J. Geophys. Res.*, *99*(B6), 11,591–11,621, doi:10.1029/94JB00042.
- Grand, S. (2002), Mantle shear-wave tomography and the fate of subducted slabs, *Philos. Trans. R. Soc. London, Ser. A*, *360*(1800), 2475–2491.
- Grand, S., R. D. van der Hilst, and S. Widiyantoro (1997), Global seismic tomography: a snapshot of convection in the Earth, *Geol. Soc. Am. Today*, *7*, 1–7.
- Hasterok, D., and D. S. Chapman (2007), Continental thermal isostasy: 2. Application to North America, *J. Geophys. Res.*, *112*, B06415, doi:10.1029/2006JB004664.
- Hatcher, R. D., Jr. (1989), Tectonic synthesis of the U.S. Appalachians, in *The Appalachian-Ouachita Orogen in the United States. The Geology of North America*, vol. F-2, edited by R. D. Hatcher Jr., W. A. Thomas, and G. W. Viele, pp. 511–535, Geological Soc. Am., Boulder, Colo.
- Hawkesworth, C. J., P. D. Kempton, N. W. Rogers, R. M. Ellam, and P. W. van Calsteren (1990), Continental mantle lithosphere, and shallow level enrichment process in the Earth's mantle, *Earth Planet. Sci. Lett.*, *96*, 256–268.
- Hildebrand, R. S. (2009), Did westward subduction cause Cretaceous-Tertiary orogeny in the North American cordillera?, *Geological Society of America Special Paper*, *457*, 71 pp., Geol. Soc. Am., Boulder, Colo.
- Hoffman, P. F. (1988), United plates of America, the birth of a craton: Early Proterozoic assembly and growth of Laurentia, *Annu. Rev. Earth Planet. Sci.*, *16*, 543–603.
- Hoffman, P. F. (1989a), Precambrian geology and tectonic history of North America, in *The Geology of North America—An Overview*, edited by

- A. W. Bally and A. R. Palmer, pp. 447–511, Geological Society of America, Boulder, Colo.
- Hoffman, P. F. (1989b), Speculations on Laurentia's first gigayear (2.0–1.0 Ga), *Geology*, *17*, 135–138.
- Hoffman, P. F. (1997), Tectonic genealogy of North America, in *Earth Structure: An Introduction to Structural Geology and Tectonics*, edited by B. A. van der Pluijm and S. Marshak, pp. 459–464, McGraw-Hill, New York.
- Hyndman, R. D., and T. J. Lewis (1999), Geophysical consequences of the Cordillera-craton thermal transition in southwestern Canada, *Tectonophysics*, *306*, 397–422, doi:10.1016/S0040-1951(99)00068-2.
- Iyer, H. M., and T. Hitchcock (1989), Upper-mantle velocity structure in the continental U.S. and Canada, in *Geophysical Framework of the Continental United States*, *Geol. Soc. Am. Mem.*, *172*, edited by L. C. Pakiser and W. D. Mooney, pp. 681–710, Geol. Soc. Am., Boulder, Colo.
- Jachens, R. C., and C. Moring (1990), Maps of the thickness of Cenozoic deposits and the isostatic residual gravity over basement for Nevada, *U.S. Geol. Sur. Open File Report*, *90-404*, 15 pp.
- Jachens, R. C., A. Griscom, and C. W. Roberts (1995), Regional extent of Great Valley basement west of the Great Valley, California: Implications for extensive tectonic wedging in the California Coast Ranges, *J. Geophys. Res.*, *100*, p. 12,769–12,790.
- Jordan, T. H. (1978), Composition and development of the continental tectosphere, *Nature*, *274*, 544–548.
- Jordan, T. H. (1981), Continents as a chemical boundary layer, *Phil. Trans. R. Soc. London, Ser. A*, *301*, 359–373.
- Jordan, T. H. (1988), Structure and formation of the continental tectosphere, *J. Petrol.*, *29*, 11–37.
- Kaban, M. K., and W. Mooney (2001), Density structure of the lithosphere in the southwestern United States and its tectonic significance, *J. Geophys. Res.*, *106*, 721–740, doi:10.1029/2000JB900235.
- Kaban, M. K., and P. Schwintzer (2001), Oceanic upper mantle structure from experimental scaling of  $V_s$  and density at different depths, *Geophys. J. Int.*, *147*, 199–214.
- Kaban, M. K., P. Schwintzer, and S. A. Tikhotsky (1999), Global isostatic gravity model of the Earth, *Geophys. J. Int.*, *136*, 519–536.
- Kaban, M. K., O. G. Flovenz, and G. Palmason (2002), Nature of the crust-mantle transition zone and the thermal state of the upper mantle beneath Iceland from gravity modelling, *Geophys. J. Int.*, *149*, 281–299.
- Kaban, M. K., P. Schwintzer, I. M. Artemieva, and W. D. Mooney (2003), Density of the continental roots: Compositional and thermal contributions, *Earth Planet. Sci. Lett.*, *209*, 53–69.
- Kaban, M. K., P. Schwintzer, and Ch. Reigber (2004), A new isostatic model of the lithosphere and gravity field, *J. Geod.*, *78*, 368–385.
- Karlstrom, K. E., S. S. Harlan, M. L. Williams, J. McLelland, J. W. Geissman, and K.-I. Ahall (1999), Refining Rodinia: Geologic evidence for the Australia-Western U.S. connection for the Proterozoic, *Geol. Soc. Am. Today*, *9*, 1–7.
- Karlstrom, K. E., S. S. Harlan, M. L. Williams, J. McLelland, J. W. Geissman, and K. I. Ahall (2001), Long-lived (1.8–0.8 Ga) Cordilleran type orogen in southern Laurentia, its extensions to Australia and Baltica, and implications for refining Rodinia, *Precambrian Res.*, *111*, 5–30.
- Karlstrom, K. E., J. M. Amato, M. L. Williams, M. Heizler, C. A. Shaw, A. S. Read, and P. Bauer (2004), Proterozoic tectonic evolution of the New Mexico region, in *The Geology of New Mexico: A Geologic History, New Mexico Geological Society Special Publication 11*, edited by G. H. Mack and K. A. Giles, pp. 1–34, NMGS, Albuquerque.
- Keller, G. R., K. E. Karlstrom, and G. L. Farmer (1999), Tectonic evolution in the Rocky Mountains region, 4-D images of the continental lithosphere, *Eos Trans. AGU*, *80*, 493–498.
- Langenheim, V. E., and R. C. Jachens (1996), Gravity data collected along the Los Angeles regional seismic experiment (LARSE) and preliminary model of regional density variations in basement rocks, southern California, *U.S. Geological Survey Open File Report*, *96-682*, USGS, Boulder, Colo., 25 pp.
- Li, X., and B. Romanowicz (1996), Global mantle shear velocity model developed using nonlinear asymptotic coupling theory, *J. Geophys. Res.*, *101*(B10), 22,245–22,272, doi:10.1029/96JB01306.
- Li, Z. X., S. V. Bogdanova, A. S. Collins, A. Davidson, B. De Waele, R. E. Ernst, I. C. W. Fitzsimons, R. A. Fuck, D. P. Gladkochub, J. Jacobs, K. E. Karlstrom, S. Lu, L. M. Natapov, V. Pease, S. A. Pisarevsky, K. Thrane, and V. Vernikovsky (2008), Assembly, configuration, and break-up history of Rodinia: A synthesis, *Precambrian Res.*, *160*(1/2), 179–210.
- Lowry, A. R., N. M. Ribe, and R. B. Smith (2000), Dynamic elevation of the Cordillera, western United States, *J. Geophys. Res.*, *105*(B10), 23,371–23,390, doi:10.1029/2000JB900182.
- Marone, F., and B. Romanowicz (2007), The depth distribution of azimuthal anisotropy in the continental upper mantle, *Nature*, *447*, 198–201.
- Marone, F., Y. Gung, and B. Romanowicz (2007), Three-dimensional radial anisotropic structure of the North American upper mantle from inversion of surface waveform data, *Geophys. J. Int.*, *171*, 206–222, doi:10.1111/j.1365-246X.2007.03465.x.
- McCulloh, T. H. (1967), Mass properties of sedimentary rocks and gravimetric effects of petroleum and natural-gas reservoirs, *U.S. Geol. Surv. Professional Paper*, *528-A*, 50 pp.
- Mooney, W. D. (1989), Seismic methods for determining earthquake source parameters and lithospheric structure, in *Geophysical framework of the continental United States*, *Geol. Soc. Am. Mem.*, *172*, edited by L. C. Pakiser and W. D. Mooney, pp. 11–34, AGS, Boulder, Colo.
- Mooney, W. D., and L. W. Braille (1989), The seismic structure of the continental crust and upper mantle of North America, *Geol. North Am.*, *A*, 39–52.
- Mooney, W. D., and J. E. Vidale (2003), Thermal and chemical variations in subcrustal cratonic lithosphere: Evidence from crustal isostasy, *Lithos*, *71*(2–4), 185–193.
- Mooney, W. D., G. Laske, and T. G. Masters (1998), CRUST 5.1: A global crustal model at  $5^\circ \times 5^\circ$ , *J. Geophys. Res.*, *103*, 727–747.
- Moore, E. M. (1991), The Southwest U.S.–East Antarctica (SWEAT) connection: A hypothesis, *Geology*, *19*, 425–428.
- Nettel, M., and A. M. Dziewonski (2008), Radially anisotropic shear velocity structure of the upper mantle globally and beneath North America, *J. Geophys. Res.*, *113*, B02303, doi:10.1029/2006JB004819.
- NOAA (2000), ETOPO2, Boulder, Colo.
- Oceanic Drilling Program (1994), 1994, Santa Barbara Basin, Site 893, in *Proc. Oceanic Drill. Program Initial Reports*, vol. 146, part 2, p. 45, Oceanic Drill. Program, College Station, Tex.
- Oldow, J. S., A. W. Bally, H. G. Avé Lallemant, and W. P. Leeman (1989), Phanerozoic evolution of the North American Cordillera (United States and Canada), in *The Geology of North America: An Overview*, vol. A, edited by A.W. Bally and A.R. Palmer, pp. 139–232, Geological Society of America, Boulder, Colo.
- Panasjuk, S. V., and B. H. Hager (2000), Models of isostatic and dynamic topography, geoid anomalies, and their uncertainties, *J. Geophys. Res.*, *105*(B12), 28,199–28,209, doi:10.1029/2000JB900249.
- Perry, H. K. C., D. W. S. Eaton, and A. M. Forte (2002), LITH5.0: A revised crustal model for Canada based on Lithoprobe results, *Geophys. J. Int.*, *150*, 285–294.
- Perry, H. K. C., A. M. Forte, and D. W. S. Eaton (2003), Upper-mantle thermochemical structure below North America from seismic-geodynamic flow models, *Geophys. J. Int.*, *154*, 279–299.
- Pollack, H. N., and D. S. Chapman (1977), On the regional variation of heat flow, geotherms and lithospheric thickness, *Tectonophysics*, *38*, 279–296.
- Pollack, H. N., S. J. Hurter, and J. R. Johnson (1993), Heat flow from the Earth's interior: Analysis of the global data set, *Rev. Geophys.*, *31*(3), 267–280, doi:10.1029/93RG01249.
- Poudjom Djomani, Y. H., S. Y. O'Reilly, W. L. Griffin, and P. Morgan (2001), The density structure of subcontinental lithosphere through time, *Earth Planet. Sci. Lett.*, *184*, 605–621.
- Röhm, A. H. E., R. Snieder, S. Goes, and J. Trampert (2000), Thermal structure of continental upper mantle inferred from S-wave velocity and surface heat flow, *Earth Planet. Sci. Lett.*, *181*, 395–407.
- Romanyuk, T., W. D. Mooney, and S. Detweiler (2007), Two lithospheric profiles across southern California derived from gravity and seismic data, *J. Geodyn.*, *43*(2), 274–307.
- Ross, G. M., and M. E. Villeneuve (2003), Provenance of the Mesoproterozoic (1.45 Ga) Belt basin (western North America): Another piece in the pre-Rodinia paleogeographical puzzle, *Geol. Soc. Am. Bull.*, *115*, 1191–1217.
- Sigloch, K., N. McQuarrie, and G. Nolet (2008), Two-stage subduction history under North America inferred from multiple-frequency tomography, *Nature Geosci.*, *1*, 458–462, doi:10.1038/ngeo231.
- Silver, P. G. (1996), Seismic anisotropy beneath the continents: Probing the depths of geology, *Annu. Rev. Earth Planet. Sci.*, *24*, 385–432.
- Silver, P. G., and W. W. Chan (1991), Shear-wave splitting and subcontinental mantle deformation, *J. Geophys. Res.*, *96*(B10), 16,429–16,454.
- Simpson, R. W., R. C. Jachens, R. J. Blakely, and R. W. Saltus (1986), A new isostatic residual gravity map of the conterminous United States with a discussion on the significance of isostatic residual anomalies, *J. Geophys. Res.*, *91*(B8), 8348–8372, doi:10.1029/JB091B08p08348.
- Snelson, C. M., T. J. Henstock, G. R. Keller, K. C. Miller, and A. Levander (1998), Crustal and uppermost mantle structure along the Deep Probe seismic profile, *Rocky Mountain Geology*, *33*, 181–198.
- Strakhov, V. N., T. V. Romaniuk, and N. K. Frolova (1989), Method of direct gravity problem solution for modeling of global and regional gravity anomalies, in *New Methods of Gravity and Magnetic Anomaly Interpretation*, pp. 118–235, Inst. Phys. of the Earth, Moscow, (in Russian).

- Thomas, W. A. (1989), The Appalachian-Ouachita orogen beneath the Gulf Coastal Plain between the outcrops in the Appalachian and Ouachita Mountains, in *The Appalachian-Ouachita Orogen in the United States, Geology of North America*, vol. F-2, edited by R. D. Hatcher Jr., W. A. Thomas, and G. W. Viele, pp. 537–553, Geol. Soc. Am., Boulder, Colo.
- Whitmeyer, S. J., and K. E. Karlstrom (2007), Tectonic model for the Proterozoic growth of North America, *Geosphere*, 3(4), 220–259.
- Van der Lee, S., and G. Nolet (1997a), Seismic image of the subducting trailing fragments of the Farallon Plate, *Nature*, 386, 266–269.
- Van der Lee, S., and G. Nolet (1997b), Upper mantle *S* velocity structure of North America, *J. Geophys. Res.*, 102(B10), 22,815–22,838, doi:10.1029/97JB01168.
- Vinnik, L. P., G. L. Kosarev, and L. I. Makeyeva (1984), Anisotropy of the lithosphere from observations of SKS and SKKS, *Dokl. Akad. Nauk USSR*, 278, 1335–1339 (in Russian).
- Williams, H., J. W. Monger, P. F. Hoffman, J. F. Lewry, and T. Rivers (1991), Anatomy of North America: thematic geologic portrayals of the continent, *Tectonophysics*, 187, 117–134.
- Zhao, D. P. (2004), Global tomographic images of mantle plumes and subducted slabs: Insight into deep Earth dynamics, *Phys. Earth Planetary Inter.*, 146, 3–24.
- Zhou, Y., G. Nolet, F. A. Dahlen, and G. Laske (2006), Global upper-mantle structure from finite-frequency surface-wave tomography, *J. Geophys. Res.*, 111, B04304, doi:10.1029/2005JB003677.

---

M. K. Kaban, USGS, MS 977, 345 Middlefield Rd., Menlo Park, CA 94025, USA.

W. D. Mooney (corresponding author), GeoForschungsZentrum, Telegrafenberg A17, D-14478 Potsdam, Germany. (mooney@usgs.gov)